Journal of Geosciences, 57 (2012), 3–23 DOI: 10.3190/jgeosci.112

Original paper

Multiple monazite growth in the Åreskutan migmatite: evidence for a polymetamorphic Late Ordovician to Late Silurian evolution in the Seve Nappe Complex of west–central Jämtland, Sweden

Jarosław MAJKA[1*], Yaron BE'ERI-SHLEVIN[2], David G. GEE[1], Anna LADENBERGER[1,3], Stefan CLAESSON[2], Patrik KONEČNÝ[4], Iwona KLONOWSKA[1,5]

[1] *Department of Earth Sciences, Uppsala University, Villavägen 16, 752-36 Uppsala, Sweden; jaroslaw.majka@geo.uu.se*
[2] *Laboratory for Isotope Geology, Swedish Museum of Natural History, Frescativägen 40, 114 18 Stockholm, Sweden*
[3] *Geological Survey of Sweden, Villavägen 18, 751-28 Uppsala, Sweden*
[4] *Dionýz Štúr State Geological Institute, Mlynská dolina 1, 817 04 Bratislava, Slovak Republic*
[5] *Department of Economic and Mining Geology, AGH – University of Science and Technology, Mickiewicza 30, 30-059 Kraków, Poland*
** Corresponding author*

Monazite from granulite-facies rocks of the Åreskutan Nappe in the Scandinavian Caledonides (Seve Nappe Complex, Sweden) was dated using *in-situ* U–Th–total Pb chemical geochronology (CHIME). Multi-spot analyses of a non-sheared migmatite neosome yielded an age of 439 ± 3 Ma, whereas a sheared migmatite gave 433 ± 3 Ma (2σ). Although the obtained dates are rather similar, a continuous array of single dates from *c.* 400 Ma to *c.* 500 Ma suggests possibly a more complex monazite age pattern in the studied rocks. The grouping and recalculation of the obtained results in respect to Y–Th–U systematics and microtextural context allowed distinguishing several different populations of monazite grains/growth zones.

In the *migmatite neosome*, low-Th and low-Y domains dated at 455 ± 11 Ma are considered to have grown under high-grade sub-solidus conditions, most likely during a progressive burial metamorphic event. The monazites with higher Th and lower Y yielded an age of 439 ± 4 Ma marking the subsequent partial melting event caused by decompression. The youngest (423 ± 13 Ma) Y-enriched monazite reveals features of fluid-assisted growth and is interpreted to date the emplacement of the Åreskutan onto the Lower Seve Nappe.

In the *sheared migmatite*, the high-Th and low-U (high Th/U) monazite with variable Y contents yielded an age of 438 ± 4 Ma, which is interpreted to date the partial melting event. Relatively U-rich rims on some of the monazite grains again reveal features of fluid-assisted growth, and thus their age of 424 ± 6 Ma is interpreted as timing of the nappes emplacement. These results call, however, for further more precise, isotopic (preferably ion microprobe) dating of monazite in the studied rocks.

Keywords: Scandinavian Caledonides; geochronology; monazite; partial melting; metamorphism
Received: 23 August 2011; accepted: 13 March 2012; handling editor: V. Janoušek

1. Introduction

Monazite ($LREEPO_4$) is one of the most common accessory phosphates in metamorphic, igneous and sedimentary rocks (Williams et al. 2007). Monazite often incorporates Th and U into its structure and has been used for isotopic dating (e.g., Parrish 1990; Poitrasson et al. 2000). The typically negligible amount of common Pb in the monazite lattice provides a unique opportunity for non-isotopic chemical electron microprobe (EPMA) dating (e.g., Suzuki and Adachi 1991; Montel et al. 1996; Williams et al. 2006; Suzuki and Kato 2008; Spear et al. 2009). This feature of monazite is, in many cases, the greatest advantage, because the very high spatial resolution of the EMPA allows the dating of fine-scale compositional domains (e.g., Terry et al. 2000; Dahl et al. 2005; Kohn et al. 2005; Pyle et al. 2005; Mahan et al. 2006; Krenn et al. 2009; Petrík and Konečný 2009).

Metamorphic monazite growth has been described over almost the whole P–T range from greenschist (e.g., Catlos et al. 2002) through amphibolite (Ferry 2000; Pyle and Spear 2003; Wing et al. 2003; Majka et al. 2008; Kim et al. 2009), to granulite (Bingen et al. 1996; Bea and Montero 1999; Mahan et al. 2006) and even eclogite facies (Krenn et al. 2009). Although monazite occurs over such a wide range of P–T conditions, it is not stable in some bulk compositions and parageneses (e.g. Williams et al. 2007). Monazite-in reactions, due to the prograde breakdown of allanite (and probably apatite) or vice versa, are known both from many metamorphic terrains (Bingen et al. 1996; Broska and Siman 1998; Finger et al. 1998; Ferry 2000; Wing et al. 2003; Majka and Budzyń 2006; Kim et al. 2009) and from experimental studies (Janots et al. 2007). Monazite "bloom" has also been recognized as an effect of garnet breakdown near the staurolite-in reaction (Pyle and Spear 2003; Kohn

and Malloy 2004). The growth of distinct generations under varying metamorphic conditions commonly results in zoned monazite crystals with multiple domains characterized by different trace-element compositions. The zoning pattern is thus not always a straightforward continuous core-to-rim change but it can be patchy, convolute or even inverse. Detailed definition of the various monazite domains with respect to chemistry, especially the trace-element systematics, is a key to genetic and geochronological interpretation of the host rock (Williams et al. 2007 and references therein).

In this study, we applied EPMA U–Th total Pb dating of monazite to investigate the metamorphic history of the Caledonian Seve Nappe Complex migmatites at Mt. Åreskutan (Sweden). The main goals are to compare the results with existing U–Pb zircon ages (Ladenberger et al. 2012 and unpublished data by the same authors) and to better understand the history prior to the partial melting event and after the pegmatite intrusion. *In-situ* work, along with chemical characterization of various growth domains, demonstrates the importance of monazite for deciphering the evolution of complex polymetamorphic terrains. The results are used to reconstruct metamorphic paths and the tectonic evolution of the highest grade units of the Seve Nappe Complex, at this key locality of the central Scandinavian Caledonides.

2. Geological background

2.1 Scandinavian Caledonides

The Caledonide Orogen in Scandinavia consists of an assemblage of allochthons that were thrust eastwards (present coordinates) onto the margin of Baltica in Silurian and Early Devonian (Fig. 1). Some of the nappes record Cambro–Ordovician history of subduction and Ordovician thrusting (Dallmeyer and Gee 1986). The nappe pile includes allochthons derived from the Early Paleozoic Baltoscandian Platform and foredeep basins (Lower Allochthon), the Neoproterozoic outer margin rift basins and continent–ocean transition zone (Middle Allochthon), oceanic domains (Upper Allochthon) and fragments of the Laurentian margin (Uppermost Allochthon) (Gee et al. 1985; Andréasson and Gee 2008). Metamorphic grade increases from the Lower into and through the Middle Allochthon. The highest metamorphic grade (granulite and eclogite facies) was reached in the upper parts of the Middle Allochthon in the Seve nappes, which are overlain by lower grade outboard terranes of the Köli and related nappes of island-arc and back-arc association and ophiolites (Upper Allochthon).

The Seve nappes are ductilely deformed and, in the southern parts of the Swedish Caledonides, yield evidence of Early Silurian granulite-facies metamorphism (Claesson 1982; Ladenberger et al. 2012),

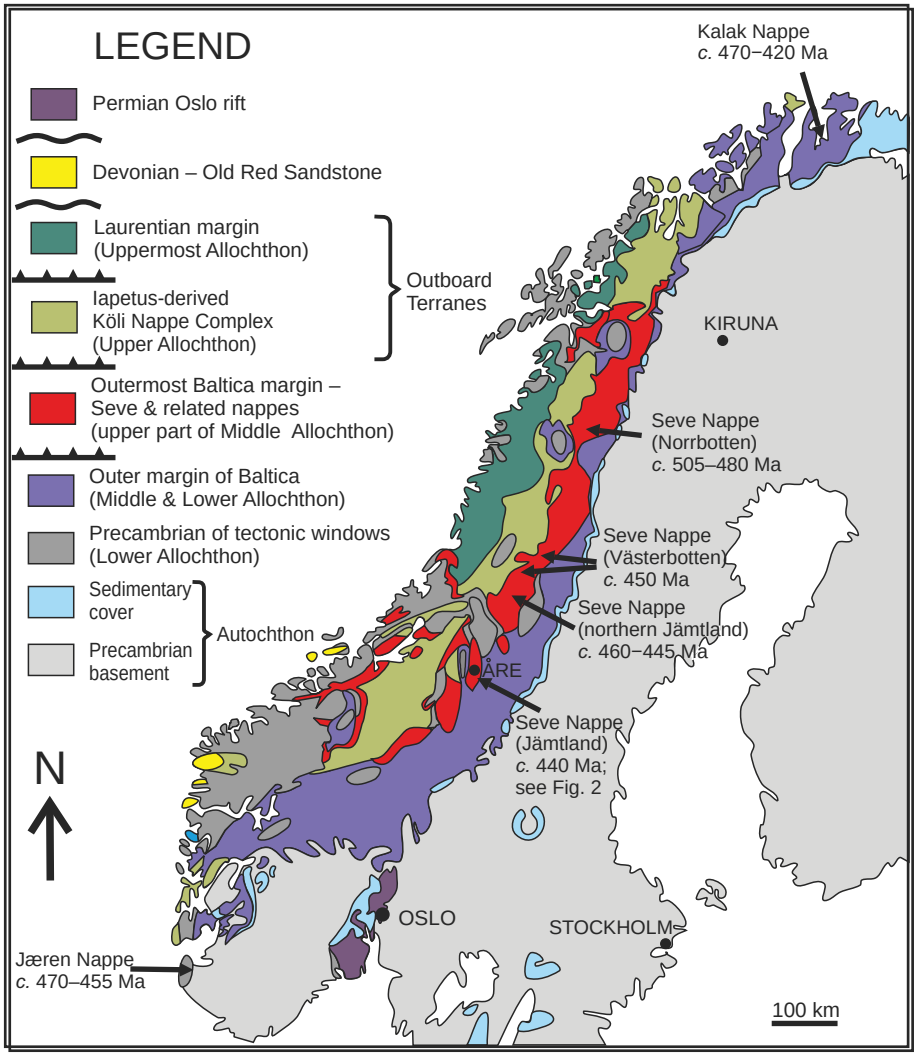

Fig. 1 Simplified tectonostratigraphic map of the Scandinavian Caledonides with geochronological data marked for Seve Nappe Complex, Kalak Nappe Complex and Jæren Nappe (Gee et al. 2010, modified).

suggesting emplacement onto the Baltoscandian Platform while still at high temperatures. This tectonothermal activity has been related to Scandian collisional orogeny and underthrusting of Laurentia by Baltica (Gee 1975). However, farther north in the orogen, in Norrbotten (Grapesvare), where the Seve nappes host abundant eclogitized dolerites (Andréasson et al. 1985; Albrecht 2000), the peak of metamorphism occurred earlier (Finnmarkian episode) with Sm–Nd garnet–whole rock ages of eclogites of *c.* 505 Ma (Mørk et al. 1988), titanite conventional U–Pb ages for calc-silicate host rocks ranging from 475 to 500 Ma (Essex et al. 1997), zircon conventional U–Pb ages on eclogites of 482 Ma (Root and Corfu 2009) and ^{40}Ar–^{39}Ar hornblende and muscovite ages of *c.* 490 and *c.* 440 Ma, respectively (Dallmeyer and Gee 1986). Apparently, subduction of the Baltoscandian outer margin in the Early Ordovician (perhaps starting in the Cambrian) with thrust emplacement of these allochthons, occurred at least 50 million years before Baltica–Laurentia collision and 80–90 m. y. prior to early Devonian eclogite-facies metamorphism in the Western Gneiss Region farther south (see also Brueckner and Van Roermund 2007). Dallmeyer and Gee (1986) related this early subduction along the outer margin of Baltica to continent–arc collision. Volcanic rocks of the lowest Köli nappes (Stephens and Gee 1985) yielded zircon U–Pb ages of 488 ± 5 Ma (Claesson et al. 1983). Emplacement of the Grapesvare eclogite-bearing allochthons was inferred to continue through the Ordovician and end in the Late Ordovician, based on ^{40}Ar–^{39}Ar muscovite cooling ages of ~440 Ma.

Within the Seve nappes south of Norrbotten, but north of northern Jämtland, the peak of metamorphism (*c.* 453 Ma) in the Seve was somewhat younger than in Norrbotten (Williams and Claesson 1987). Farther south, in northern Jämtland, Brueckner et al. (2004) and Brueckner and Van Roermund (2007) obtained 458 ± 4 Ma Sm–Nd ages on eclogites and garnet peridotites and Root and Corfu (2009) 446 ± 1 Ma zircon U–Pb ages on eclogite. These data suggest that subduction along the Baltoscandian margin may have continued throughout the Ordovician and culminated – at least in southern areas – during the Early Silurian Baltica–Laurentia collision.

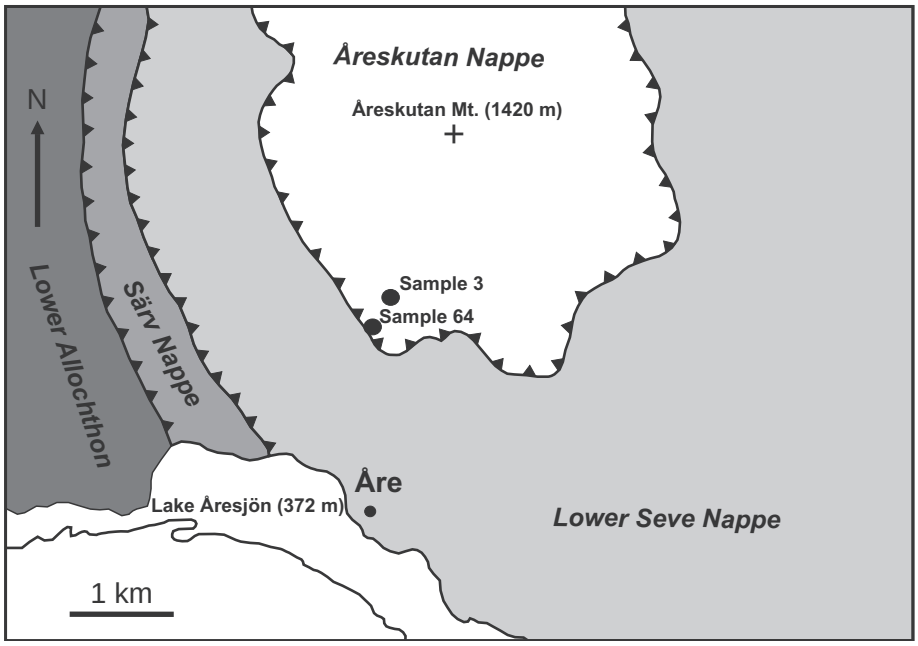

Fig. 2 Geological map of the Åre area with locations of samples 3 and 64 marked.

2.2 Seve nappes in west-central Jämtland

The presence of granulite-facies gneisses of the Seve nappes in the open Åre Synform of western Jämtland (Figs 1–2), thrust over highly deformed coral and crinoid-bearing limestones and other low greenschist-facies sedimentary formations of the Lower Allochthon, was recognized in the late nineteenth century (Törnebohm 1888), establishing Mt. Åreskutan as one of the classical localities for the study of thrust tectonics. For nearly a hundred years, these migmatized gneisses were thought to be of Precambrian age, though clearly subjected to intense Caledonian deformation and, at least, low-grade metamorphism. Conventional U–Pb zircon dating (Claesson 1982, 1987) and subsequent ion microprobe studies (Williams and Claesson 1987; Tab. 1), demonstrated that the high-grade metamorphism is Silurian, whereas various older cores in zircon of the paragneisses have Precambrian, mainly Mesoproterozoic, ages. Later studies of the high-grade Seve Nappes farther west in Jämtland on Snasahögarna (Gromet et al. 1996; Tab. 1) confirmed the Silurian ages with U–Pb dating of monazite in the granulite facies gneisses at 440–435 Ma. Recent ion microprobe analysis of zircon from the Åreskutan migmatites yielded an age of 442–436 Ma (early Llandovery) for the peak of metamorphism (Ladenberger et al. 2012; Tab. 1).

Migmatites on the top of the Mt. Åreskutan pass downward into a high-grade shear zone and mylonite units (Helfrich 1967; Yngström 1969), which separate them from the underlying amphibolite-facies Lower Seve

Tab. 1 Previous U–Pb dating results from the Åre area

Unit	Method	Age (Ma)	Reported error (± 2σ)	Reference
Åreskutan Nappe (leucogranite)	U–Pb zircon ion microprobe	441	10	Williams and Cleasson (1987)
Åreskutan Nappe (granulite-facies gneiss)	U–Pb monazite TIMS	440–435	–	Gromet et al. (1996)
Lower Seve Nappe at Åreskutan Mt.	U–Pb titanite TIMS	437–427	–	Gromet et al. (1996)
Åreskutan Nappe (leucogranite)	U–Pb zircon ion microprobe	442	5	Ladenberger et al. (2012)
Åreskutan Nappe (migmatite)	U–Pb zircon ion microprobe	441	4	Ladenberger et al. (2012)
Åreskutan Nappe (leucocratic segregation in mafic paleosome)	U–Pb zircon ion microprobe	436	2	Ladenberger et al. (2012)
Åreskutan Nappe (pegmatite)	U–Pb zircon ion microprobe	430	3	Ladenberger et al. (2012)

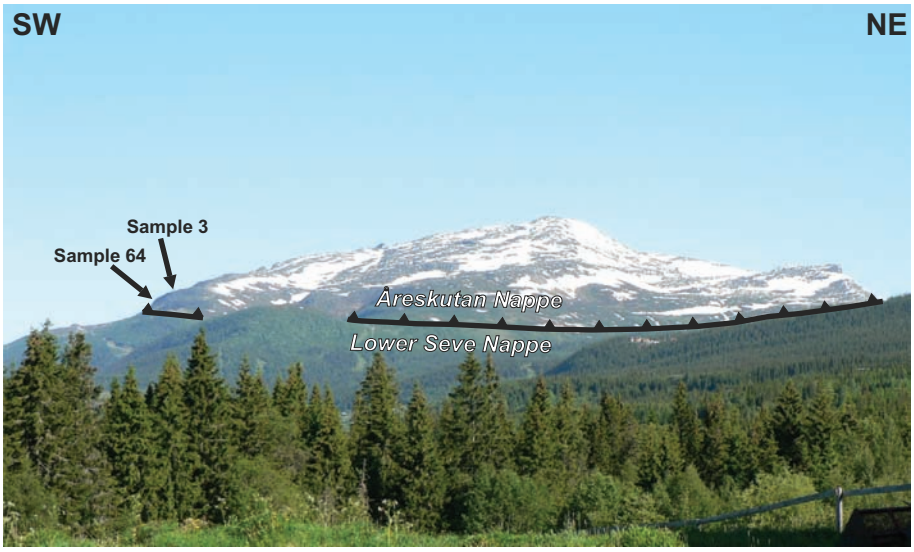

Fig. 3 View of Mt. Åreskutan from the southeast.

Nappe (Fig. 3). The parageneses of the Åreskutan migmatites have been described by Arnbom (1980) and Arnbom and Troëng (1982). The neosomes are dominated by quartz, K-feldspar, plagioclase, sillimanite and/or kyanite, garnet, biotite and cordierite. The paleosome consists of two main components, pelitic gneiss and mafic rock, with the former having a similar, but less felsic mineralogy than the neosome and the latter containing both ortho- and clinopyroxene, hornblende, garnet and plagioclase. Early foliations are commonly present in the paleosome, providing an evidence of deformation and metamorphism prior to migmatization. A younger foliation is usually present in the neosome and it increases in intensity towards the base of the nappe and towards the basal shear zone. Concordant elongate bodies of leucogranite, up to about 20 m thick, occur within the migmatites. Abundant pegmatite veins clearly truncate the younger foliation within the migmatites, but not the mylonites at the base of the nappe. The basal shear zone is developed over a thickness of *c*. 50 m with the upper parts having parageneses generally similar to the overlying pelitic gneisses and neosome. In addition, they contain a second generation of generally smaller, idiomorphic garnet. Gromet et al. (1996) demonstrated that titanite in calc-silicate-rich psammitic metasedimentary units of the Lower Seve Nappe, directly beneath this shear zone at the base of the Åreskutan Nappe, also recorded early to mid-Silurian ages (437–427 Ma; Tab. 1).

2.3 Samples for monazite electron-microprobe analysis

To investigate the metamorphic events recorded within the Åreskutan Nappe migmatites and relate these to the possible effects of thrusting of the unit on top of the Lower Seve Nappe, samples were collected from within the basal shear zone and upwards into the nappe. These included: (1) a neosome of a non-sheared migmatite (sample 3) located about 100 m above the basal shear zone, and (2) a sheared migmatite (sample 64) from within the basal shear zone, *c*. 30 m above the mylonitic contact to the underlying nappe (Figs 2–3). Notably, ion microprobe U–Pb dating of zircon from sample 3 yielded an age of 442 ± 3 Ma (Ladenberger et al. 2012), timing the main migmatization event in the nappe.

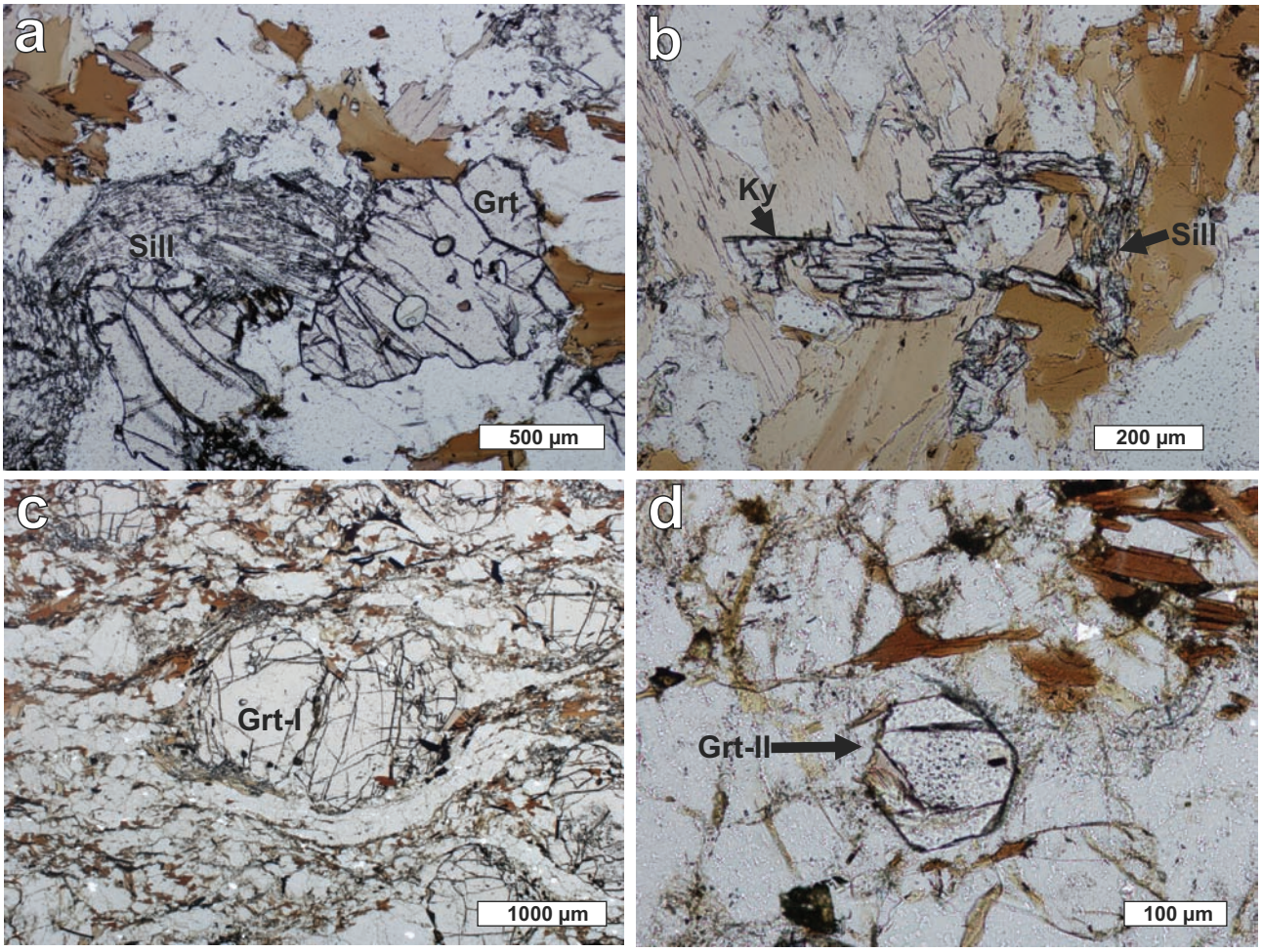

Fig. 4 Photomicrographs of (**a**) garnet porphyroblast partially replaced by sillimanite in migmatite neosome (sample 3), (**b**) kyanite partially replaced by sillimanite in migmatite neosome (sample 3), (**c**) deformed porphyroblast of earlier garnet generation in sheared migmatite (sample 64) and (**d**) euhedral garnet of second generation in sheared migmatite (sample 64).

2.3.1 Migmatite neosome (sample 3)

The sample is a reddish garnet–sillimanite migmatitic paragneiss with well-developed melanosome and leucosome domains. The layered fabric is intensively folded indicating movement top to the east. The rock contains numerous leucocratic veinlets composed mostly of quartz and plagioclase, which postdated the main foliation and flow structures in the host rock. A typical feature is the occurrence of a wide range of garnet sizes, from a few millimeters to several centimeters in diameter. Garnet grains dominate biotite–sillimanite-rich layers (melanosome) and show evidence of retrogression, such as resorption microtextures or sillimanite and biotite coatings (Fig. 4a). Garnet is commonly deformed and rotated. Garnet porphyroblasts contain inclusions of quartz, biotite, muscovite, monazite, sillimanite and, rarely, kyanite. Kyanite occurs also in the matrix (Fig. 4b) and is commonly overgrown by tiny sillimanite. Biotite, quartz, sillimanite, muscovite and titanite are also observed in cracks within the garnet. Leucosome layers are mainly composed of plagioclase (albite–oligoclase) and quartz mosaic. K-feldspar is scarce and represented by microcline, typically with visible twinning. Rare myrmekitic intergrowths of quartz and plagioclase are also found. Quartz, sillimanite and biotite locally form symplectites. Accessory minerals are represented by titanite, apatite, zircon, monazite (usually as inclusions in biotite and quartz) and epidote (scarce). Later alteration processes are expressed by the presence of sericite and calcite in plagioclase as well as chloritization of biotite and garnet.

2.3.2 Sheared migmatite (sample 64)

This mylonitic migmatite gneiss exhibits a strong penetrative flat-lying foliation. The composition is similar to sample 3, but with thinner layers ($\leq$ 5 mm) of melanosome and leucosome and superimposed mylonitic fabrics. Garnet occurs in the melanosome where it is

generally smaller than in migmatites located further up in the section (e.g., sample 3). Two main generations of garnet are distinguished: (1) older, relatively large anhedral porphyroblasts up to several centimeters across with inclusions and fractures; the garnet grains rotated and commonly exhibit embayed shapes indicating syn-kinematic resorption or retrogression (Fig. 4c) and (2) younger, smaller euhedral porphyroblasts up to 1 mm in diameter, which usually contain fewer inclusions than the larger grains (Fig. 4d). The variety of inclusions in garnet includes biotite, quartz, zircon, monazite, apatite, and sillimanite. Biotite and sillimanite also grew in pressure shadows of larger garnet grains. Sillimanite occurs in two forms, as larger euhedral grains and in aggregates of anhedral small grains within higher strain zones. The leucosome is dominated by a recrystallized mosaic of quartz, plagioclase (albite–oligoclase) and occasionally K-feldspar (microcline). Myrmekites of quartz and plagioclase are present. A characteristic feature of this mylonitic migmatite is the presence of graphite which, along with biotite and sillimanite, defines the foliation. Accessory minerals are: titanite, rutile, zircon, monazite (mostly in matrix, but found also in garnet), and epidote. Kyanite has not been found in thin section, but has been observed in a hand specimen. Secondary alteration is indicated by sericitization of plagioclase.

3. Methods

3.1 Analytical conditions

Electron-microprobe dating and chemical characterization of monazite grains was performed using a Cameca SX-100 electron microprobe housed at the Department of Electron Microanalysis at the Dionýz Štúr State Geological Institute (Geological Survey) in Bratislava, Slovak Republic. 180 nA beam current and 15 kV accelerating voltage were used with a beam diameter of 1 to 3 μm. Background level was determined using a linear fit. The counting time (peak + background) for Si, Al, Ca, P and As was 20 s, for REE 25 s, for Th and Y 35 s, for U 65 s and for Pb 150 s. The following standards were used: Si – wollastonite, Al – Al_2O_3, Ca – wollastonite, Pb – PbS, Th – ThO_2, U – UO_2, P – apatite, As – $GaAs_2$, S – pyrite, Fe – fayalite, Sr – $SrTiO_3$, REE and Y – REE and Y phosphates. Si, Al, As were measured with the use of a TAP crystal; Ca, Pb, U, Th, Y, P on LPET and REE on LLIF crystals. The following analytical lines were utilized: K_α for Si, Al, Ca, P, Fe, Sr and S, L_α for La, Ce, Gd, Tb, Tm, Yb, Y and As, and L_β for Pr, Nd, Sm, Eu, Dy, Ho, Er and Lu. In order to determine concentrations of Pb and Th, M_α line was used, whereas determination of U was performed with M_β spectral line. PAP corrections (Pouchou and Pichoir 1985) were applied throughout. All errors reported, depicted, and discussed in this paper are at the 2σ level (95% confidence limits).

Monazite analyses are usually complicated by peak overlaps among various elements. Intra-REE interferences were avoided in part by selection of L_β lines. Other peak overlaps were corrected for by empirically derived correction factors (*Cf*, after Pyle et al. 2002). Interferences, harmful for age determination, on PbM_α (by Y $L_{\gamma 2,3}$), UM_β (by ThM_γ, ThM_3–N_4, and ThM_5–P_3), and PbM_α (by $ThM_{\zeta 1}$ and $ThM_{\zeta 2}$) were also resolved by *Cf*. Monazite was analysed during two sessions. The calibrations of Pb–Th–U–Y were refreshed at the beginning of both. The *Cf* factors were derived concurrently with each new calibration. Background intensity, measured at two points located on both sides of the PbM_α line, was used for the linear background correction. This leads to a potential deficiency in Pb net counts, given the curved (exponential) nature of the background in vicinity of the PbM_α peak (Jercinovic and Williams 2005). The Pb deficiency is further corrected for by linear regression of some 100 chemical spot analyses of five monazite age standards. The resulting factor delta Pb includes the requisite correction for the Pb deficiency mentioned above. Representative compositional analyses of different types of dated monazites are presented in Tab. 2.

X-ray maps of the selected monazite grains were collected using a Cameca SX-50 electron microprobe in the National Microprobe Laboratory at the Department of Earth Sciences, Uppsala University, Sweden. For X-ray maps, an accelerating voltage of 20 kV and a beam current of 50 nA were used.

3.2 Dating strategies and age calculations

Chemical monazite dating strategies have been categorized into two types: "top-down" and "bottom-up" (Dahl et al. 2005; Williams et al. 2006). The first invokes the traditional pseudo-isochron method of Suzuki and Adachi (1991) as well as the age histogram method of Montel et al. (1996). "Top-down" methods are based on collection of a large number of analytical spots from many individual domains/crystals in single or even multiple samples. Subsequently, a statistical analysis is used for the age calculation.

According to the "bottom-up" dating strategy (Williams et al. 2006, 2007), detailed analyses of previously characterized compositional domains (by X-ray compositional mapping) should be carried out. Subsequently, the geological meaning of the obtained dates is interpreted as a function of monazite chemistry, textural and structural context and statistical arguments.

The dating routine used in this study basically followed that of Konečný et al. (2004), recently revised

Tab. 2 Representative chemical analyses of different monazite types dated in this study (wt. % and apfu)

wt. %	A*	B	C	D	E
P_2O_5	28.56	31.06	30.41	28.18	28.53
PbO	0.05	0.08	0.10	0.14	0.16
ThO_2	2.45	4.30	4.72	3.71	3.73
UO_2	0.18	0.19	0.32	1.30	1.70
Y_2O_3	0.20	0.33	2.49	1.25	0.37
La_2O_3	15.07	13.46	13.97	12.89	13.87
Ce_2O_3	30.73	29.53	27.69	27.71	29.19
Pr_2O_3	3.56	3.50	3.08	3.24	3.32
Nd_2O_3	13.49	13.53	11.24	13.08	12.77
Sm_2O_3	2.38	1.24	2.03	2.52	2.27
Eu_2O_3	0.07	n.d.	0.17	0.32	0.03
Gd_2O_3	1.18	1.32	1.52	1.79	1.35
Tb_2O_3	0.03	0.07	0.14	0.10	0.09
Dy_2O_3	0.11	0.14	0.66	0.51	0.17
Ho_2O_3	n.d.	n.d.	0.06	n.d.	n.d.
Er_2O_3	0.30	0.32	0.47	0.38	0.34
Tm_2O_3	0.06	0.19	0.06	0.12	0.04
Yb_2O_3	0.12	0.13	0.15	0.15	0.09
Lu_2O_3	0.11	n.d.	0.08	0.06	0.07
FeO	n.d.	n.d.	n.d.	n.d.	0.04
SO_3	0.02	n.d.	0.03	0.15	0.02
CaO	0.56	0.89	1.05	1.17	1.10
SrO	n.d.	0.01	0.04	n.d.	n.d.
Al_2O_3	n.d.	n.d.	n.d.	n.d.	n.d.
SiO_2	0.18	0.24	0.23	0.33	0.28
As_2O_5	0.17	n.d.	0.15	0.15	0.16
Total	99.60	100.53	100.86	99.25	99.67

apfu (based on 24 O)					
P	5.824	6.067	5.950	5.755	5.809
Pb	0.003	0.005	0.006	0.009	0.010
Th	0.134	0.226	0.248	0.203	0.204
U	0.010	0.010	0.016	0.070	0.091
Y	0.026	0.041	0.306	0.160	0.047
La	1.339	1.146	1.191	1.147	1.230
Ce	2.710	2.495	2.343	2.447	2.570
Pr	0.312	0.294	0.259	0.284	0.291
Nd	1.160	1.115	0.928	1.127	1.097
Sm	0.198	0.099	0.162	0.210	0.188
Eu	0.006	0.000	0.014	0.027	0.002
Gd	0.095	0.101	0.116	0.143	0.107
Tb	0.002	0.005	0.011	0.008	0.007
Dy	0.009	0.010	0.049	0.039	0.013
Ho			0.005		
Er	0.023	0.023	0.034	0.029	0.025
Tm	0.004	0.014	0.004	0.009	0.003
Yb	0.009	0.009	0.011	0.011	0.007
Lu	0.008		0.006	0.004	0.005
Fe			0.000		0.008
S	0.004		0.005	0.027	0.003
Ca	0.144	0.220	0.261	0.301	0.283
Sr		0.001	0.005		
Al					
Si	0.044	0.055	0.052	0.080	0.068
As	0.021		0.018	0.019	0.020
Total	12.085	11.934	12.001	12.110	12.090

n.d. – not detected
*migmatite neosome: A – Th-poor zone, B – Th-rich zone, C – Y-rich zone
sheared migmatite: D – Y-rich core of grain enclosed in garnet, E – U-rich rim of grain enclosed in garnet

in Petrík and Konečný (2009). According to this dating protocol, we have imaged all monazite grains with backscattered electrons (BSE) to identify and delimit different compositional domains. Subsequently, we have selected most representative grains for dating. These were covered by as many analytical spots as possible ensuring that none of the spots straddled boundaries between neighboring domains. According to Williams et al. (2006) such a "top-down" dating strategy can be satisfactory when the dated grains are large enough and show well visible growth or sector zones. Here, we considered first the "top-down" strategy for a large number of grains. Then we recalculated ages for all grains according to the "bottom-up" strategy similar to that of Williams et al. (2006) in order to further constrain the age variation and its relation to the composition of the dated domains.

Age results are based on the weighted histogram method of Montel et al. (1996) whereby model dates calculated for each spot analysis are presented in an age histogram. Subsequently all model dates are processed together and weighted average ages are calculated. The age calculation was performed using the Microsoft Excel add-in program DAMON (Konečný et al. 2004) which reads the data, calculates model dates and weighted average ages, and constructs histograms with pseudo-isochrons.

4. Y–Th–U systematics and monazite growth

Considering the pelitic protolith of the Åreskutan migmatites, the Y and Th systematics in monazite may be crucial for defining their metamorphic evolution (e.g. Terry et al. 2000; Pyle and Spear 2003; Dahl et al. 2005; Kohn et al. 2005; Pyle et al. 2005). Monazite in low- and middle-grade rocks incorporates Th via Rayleigh-like fractionation (Kohn and Malloy 2004); with the increasing temperatures, the Th content typically decreases, though. In absence of prograde xenotime and/or allanite, the Y partitioning is mainly governed by reactions involving garnet (e.g., Pyle and Spear 2003; Högdahl et al. 2012). Zhou and O'Nions (1999) showed that monazite growing after garnet-in reactions will contain rather low Y + HREE concentrations. The

behavior of monazite during migmatization is, however, still not well understood. This mineral may grow directly from the melt, or form due to final melt crystallization (see also Högdahl et al. 2012). Notwithstanding this problem, a general trend of increasing Y content from initial melting up to melt crystallization has been observed (Kohn et al. 2005). Given this, the youngest monazite should be the richest in Y, which is a consequence of garnet consumption during melting or post-crystallization retrogression during cooling. The Th/U ratio may be also used to discriminate among various monazite generations from the same migmatite sample (e.g., Bea and Montero 1999). This ratio is probably independent of chemical reactions involving monazite and garnet and should hence decouple from Y partitioning, which is strongly connected with garnet stability. Bea and Montero (1999) noticed that monazite newly grown in equilibrium with melt has significantly higher Th/U ratios than the previous metamorphic monazite generation. The authors interpreted this to reflect the increased partitioning of U into the melt.

5. Back-scattered electron images and chemical zoning of monazite from Mt. Åreskutan

5.1 Migmatite neosome

Monazite in this lithology occurs as grains exhibiting: (1) concentric zoning in the BSE images, with the cores darker and usually Th-poorer than the rims, (2) sector zoning, whereby the central zones are usually Th-poorer than the rims, and (3) patchy zoning, with no apparent correlation between the chemistry and geometric position of the given zone (Fig. 5a–c).

In most cases, monazite shows normal core–rim zoning with Th-depleted core and Th-enriched, commonly composite rim (Fig. 6a). The Th-poor cores, characterized by the lowest Th/U ratios, are thought to reflect sub-solidus pre-melting, prograde growth. High Th rims, with higher Th/U ratios suggestive of growth in equilibrium with melt, are evident in most of the dated grains. Interestingly, these do not show substantial variations in the, generally low, Y contents. Such low-Y zones presumably developed in the garnet stability field. Similar trends are visible in chemistry of the grains exhibiting sector zoning. In case of one grain (Fig. 6b), peculiar cloudy core was observed with relatively high Y and slightly elevated U contents. The cloudy Y-enriched core extends from the grain boundary towards its center. A closer look at neighboring phases reveals that this high-Y zone has developed only at a place where the monazite was in contact with biotite. We suggest that this phyllosilicate played a role as a fluid channel, a feature commonly observed in other metamorphic rocks (e.g., Poitrasson et al. 2000; Majka and Budzyń 2006). Indeed the chemistry of this zone indicates most probably a late, sub-solidus growth, induced by fluids. Additionally, the presence of a tiny inner core (being probably an equivalent of the inner rim; see Fig. 6b) entrapped in the cloudy outer core may suggest fluid-induced dissolution–reprecipitation of this part of monazite. Inner rim and inner core (tiny zone mentioned above) in this grain are characterized by Th and Y values similar to the outer zones in normally-zoned monazites. Additional U-enriched outermost discontinuous rim is also visible in this grain.

5.2 Sheared migmatite

Back-scattered electron (BSE) imaging and spot analyses revealed that monazite in this lithology shows two types of internal zoning: (1) continuous normal zoning with Th content increasing rimwards (Fig. 5d), only sometimes slightly decreasing in the outermost rims and (2) discontinuous core to rim zoning, whereby the cores enriched in Th and slightly in U are surrounded by a Th-rich domain, which is then enclosed by rather Y-poor and clearly U-enriched rim. Notably, such monazites occur as inclusions in garnets (Fig. 5e–f).

Typical examples of these two monazite varieties were mapped chemically (Fig. 6c–d). The inner core of the matrix grain showing core–rim zoning (Fig. 6c) is Th- and Y-poor, which is indicative of a sub-solidus growth, probably pre-dating the partial melting. The outer core and rim of this grain, both characterized by high Th contents (and Th/U ratios) and low Y, have been most probably growing in equilibrium with the melt. Monazite shown on Fig. 6d exhibits a core characterized by relatively low Th and high U at relatively high Y contents. Its low Th/U and elevated Y may indicate either a sub-solidus growth or an effect of garnet consumption at a very early stage of melting. Such a pattern of Th/U vs. Y in monazite incorporating Y from resorbed garnet in granulite-facies migmatites was reported by Hermann and Rubatto (2003). Recent thermodynamic modeling of garnet–monazite interaction by Spear and Pyle (2010) suggested that coexistence of sharply Y-contrasting and simultaneously crystallizing monazite domains may occur in a high-grade rock due to diffusion of Y between garnet and monazite. Importantly, the studied grain is enclosed within garnet and thus the interaction with the host mineral seems likely.

The outer strongly U-enriched rim of this grain reflects most probably a post-melt crystallization induced by late metamorphic fluids. The grain is connected with the matrix via cracks in the garnet, providing a possible path for such a fluid infiltration. Relatively low Y con-

tent suggests growth in presence of a stable garnet (of second generation, see also Fig. 4d). Similar, partially altered monazites that are known from previous works (e.g. Terry et al. 2000) were recently experimentally grown by Harlov and Hetherington (2010 and citations therein).

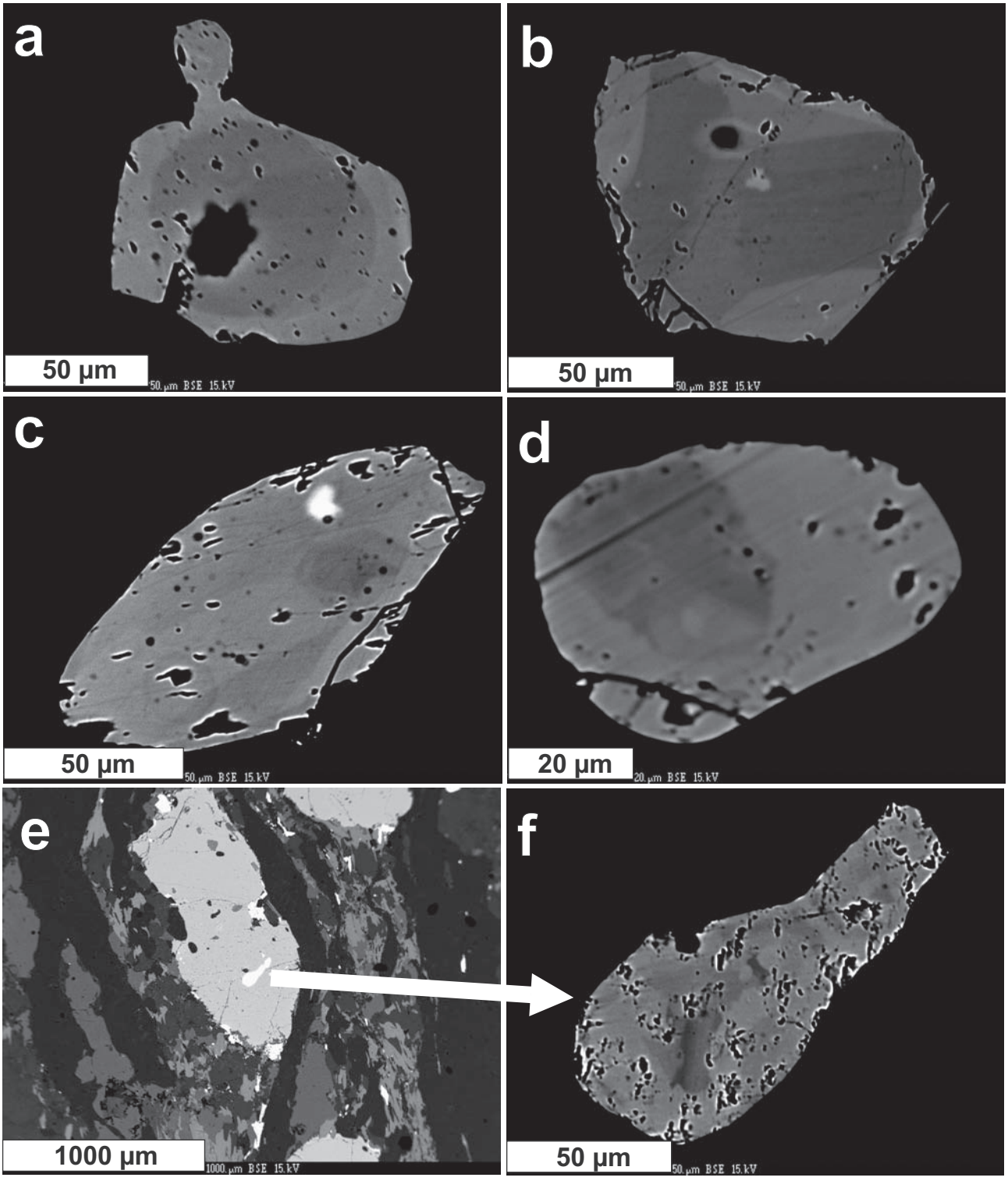

Fig. 5 Back-scattered electron (BSE) images of different zoning patterns in the studied monazites. Monazite in migmatite neosome (sample 3) features normal (**a**), sector (**b**), or patchy (**c**) zoning. The grains in sheared migmatite (sample 64) reveal usually simple two-fold normal zoning (**d**), but those enclosed in Grt-I porphyroblasts (**e**) show more complicated core-to-rim zoning pattern (**f**).

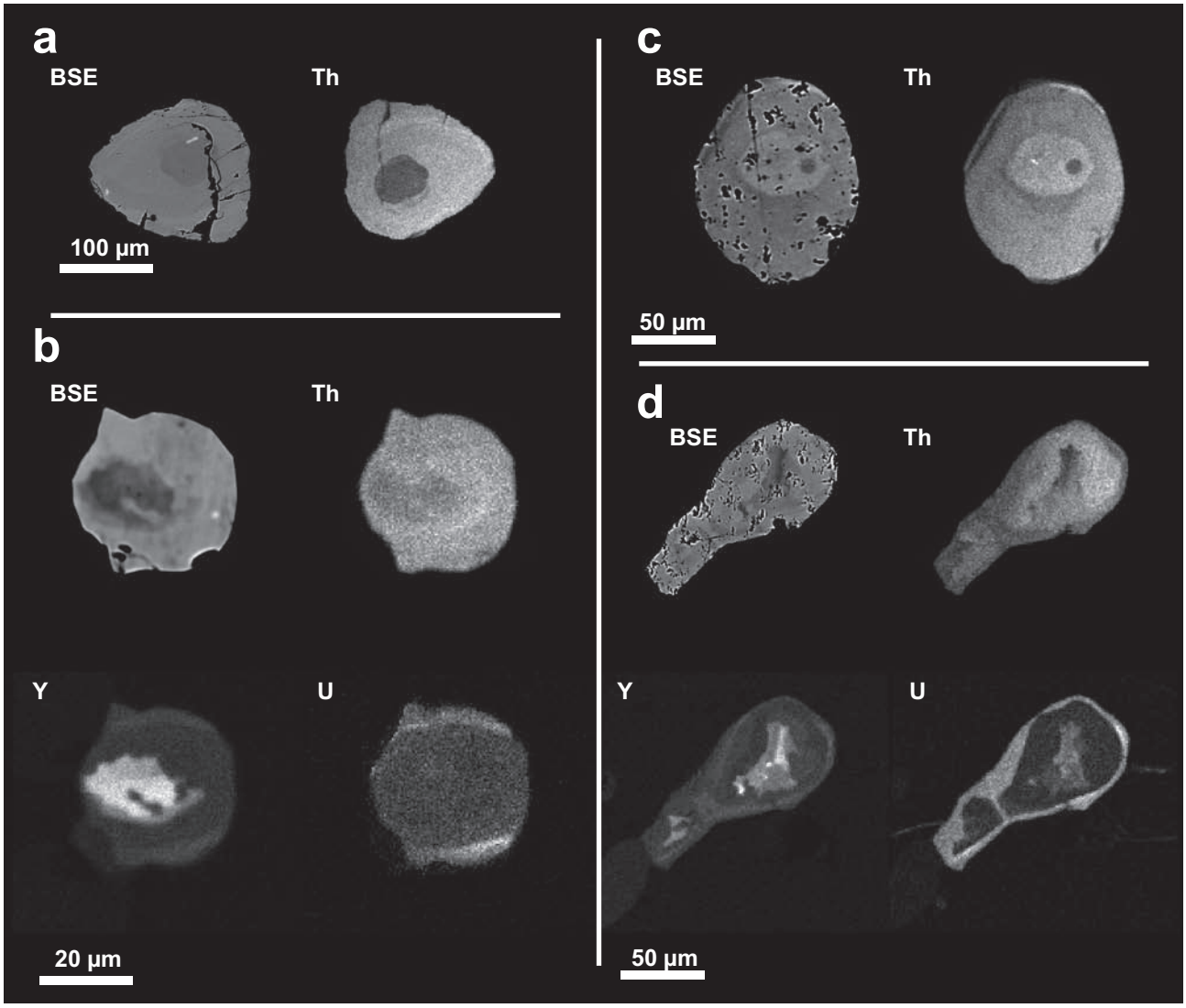

Fig. 6 Back-scattered electron (BSE) images and Th, Y, U chemical maps (light = high and dark = low concentrations) of selected monazite grains. (**a**) monazite 3–5 with a Th-depleted core that presumably recorded of the early burial metamorphism, whereas the two outer rims enriched in Th reflect partial melting stage; (**b**) monazite 3–7, the two Th-enriched domains of which could have grown at the partial melting stage, whereas the cloudy, Y-enriched core (reconstituted) originated probably during the nappe emplacement; (**c**) monazite 64–1, where the tiny Th-depleted core may have recorded the burial metamorphism, whereas the inner and outer rims are formed by Th-enriched monazite typical of partial melting; (**d**) monazite 64–4, where the two Y- and Th-enriched core domains reflect partial melting, whereas reconstituted U-enriched "rim" has been formed during nappe emplacement. Monazites 3–5 and 64–1 did not show any specific Y and U zoning patterns.

6. Dating results

6.1 Multi-spot dating ("top-down" approach)

Electron-microprobe single spot model dates from both migmatite neosome (sample 3; n = 118 on 8 grains in one thin section) and sheared migmatite (sample 64; n = 149 on 11 grains in two thin sections) are presented in Tab. 3. Regardless of being characterized by normal zoning or patchy texture, one significantly darker and up to two brighter zones are visible in all grains. Calculation of all model dates yielded weighted averages of 439 ± 3 Ma (n = 118, MSWD = 1.17, probability – p = 0.1) for migmatite neosome (sample 3) and 433 ± 3 Ma (n = 149, MSWD = 1.08, p = 0.24) for sheared migmatite (sample 64). However, a nearly continuous array of dates from 400 to 500 Ma is visible, suggesting the presence of monazite domains of distinct ages.

Although the obtained weighted average ages are not in conflict with the geological context and previous dating results from the same locality, the associated low probability values, composite internal zoning of monazite and the very large spread of single dates all suggest that rather than representing single meaningful geologic events (at *c.* 433 and 439 Ma), these averages represent mixed ages of several monazite generations, possibly

Tab. 3 Measured Th, U, Pb concentrations, Th* values, ages and 1 sigma errors for dated monazite samples 3 (AL07003) and 64 (AL08064)

Analysis number	Sample	Th (wt. %)	U (wt. %)	Pb (wt. %)	Y (wt. %)	Th (1σ)	U (1σ)	Pb (1σ)	Age (Ma)	Error (Ma)	Th*	Th/U
1	3	1.6032	0.1818	0.0427	0.3871	0.0112	0.0060	0.0026	434	30.9	2.20	8.82
2	3	1.6515	0.1820	0.0503	0.3538	0.0114	0.0060	0.0026	499	30.8	2.25	9.07
3	3	1.6519	0.1875	0.0460	0.3612	0.0114	0.0061	0.0026	453	30.2	2.27	8.81
4	3	1.7247	0.1854	0.0495	0.3279	0.0116	0.0060	0.0026	473	29.5	2.33	9.30
5	3	1.7725	0.1005	0.0443	0.2787	0.0117	0.0059	0.0026	470	32.4	2.10	17.63
6	3	1.8005	0.0924	0.0421	0.2830	0.0118	0.0059	0.0026	447	32.1	2.10	19.48
7	3	1.9310	0.1471	0.0480	0.1579	0.0122	0.0059	0.0026	444	28.0	2.41	13.13
8	3	1.9494	0.1612	0.0511	0.1784	0.0123	0.0060	0.0026	460	27.7	2.48	12.09
9	3	1.9612	0.1836	0.0472	0.1863	0.0123	0.0060	0.0026	412	26.5	2.56	10.68
10	3	2.0978	0.1656	0.0505	0.1533	0.0127	0.0060	0.0026	428	25.8	2.64	12.67
11	3	2.1240	0.1615	0.0565	0.1629	0.0128	0.0060	0.0026	475	26.1	2.65	13.15
12	3	2.1332	0.1917	0.0559	0.1656	0.0127	0.0059	0.0026	452	24.6	2.76	11.13
13	3	2.1537	0.1616	0.0518	0.1569	0.0128	0.0059	0.0025	431	24.8	2.68	13.33
14	3	2.1816	0.1845	0.0579	0.1645	0.0130	0.0060	0.0026	464	24.5	2.79	11.82
15	3	2.1984	0.1313	0.0572	0.3386	0.0130	0.0059	0.0026	485	26.4	2.63	16.74
16	3	2.2739	0.1719	0.0600	0.1696	0.0133	0.0060	0.0026	472	24.4	2.84	13.23
17	3	2.2838	0.1707	0.0601	0.1800	0.0134	0.0060	0.0026	472	24.4	2.84	13.38
18	3	2.5674	0.1523	0.0619	0.1780	0.0143	0.0061	0.0027	450	23.0	3.07	16.86
19	3	2.6146	0.1309	0.0595	0.3515	0.0144	0.0060	0.0026	437	22.8	3.04	19.98
20	3	2.7760	0.1454	0.0690	0.1631	0.0149	0.0060	0.0026	473	21.7	3.25	19.09
21	3	2.7913	0.1631	0.0652	0.1858	0.0150	0.0061	0.0027	438	21.2	3.33	17.11
22	3	2.8662	0.1854	0.0706	0.1752	0.0152	0.0060	0.0026	454	20.2	3.47	15.46
23	3	4.2800	0.1048	0.0905	0.0328	0.0197	0.0059	0.0027	437	15.5	4.62	40.86
24	3	4.7166	0.1153	0.0915	0.0415	0.0211	0.0059	0.0027	401	13.9	5.09	40.91
25	3	4.7237	0.1095	0.0997	0.0424	0.0211	0.0059	0.0027	438	14.1	5.08	43.14
26	3	4.7772	0.1161	0.1005	0.0457	0.0213	0.0059	0.0027	435	13.9	5.16	41.15
27	3	4.5731	0.1101	0.1012	0.0471	0.0206	0.0059	0.0027	458	14.6	4.93	41.55
28	3	4.7750	0.1074	0.1001	0.0486	0.0212	0.0059	0.0026	436	13.9	5.13	44.46
29	3	4.7587	0.1031	0.0992	0.0497	0.0212	0.0059	0.0027	434	14.1	5.10	46.16
30	3	4.2245	0.1179	0.0958	0.0498	0.0196	0.0060	0.0027	463	15.8	4.61	35.83
31	3	4.6627	0.1114	0.0994	0.0508	0.0209	0.0060	0.0027	441	14.3	5.03	41.85
32	3	4.2684	0.1690	0.0999	0.0515	0.0197	0.0060	0.0026	462	14.8	4.82	25.26
33	3	4.3903	0.1169	0.0935	0.0563	0.0201	0.0060	0.0027	437	15.0	4.77	37.56
34	3	3.1761	0.2384	0.0744	0.0734	0.0161	0.0060	0.0025	420	16.8	3.96	13.32
35	3	4.0393	0.1841	0.0899	0.0767	0.0188	0.0060	0.0026	432	15.0	4.64	21.94
36	3	3.9846	0.2250	0.0882	0.0804	0.0188	0.0061	0.0027	418	15.0	4.72	17.71
37	3	3.9467	0.1962	0.0962	0.0819	0.0186	0.0061	0.0026	468	15.5	4.59	20.11
38	3	4.0390	0.2386	0.0920	0.0839	0.0189	0.0061	0.0026	426	14.6	4.82	16.92
39	3	3.9512	0.2179	0.0873	0.0846	0.0186	0.0061	0.0026	418	15.0	4.66	18.14
40	3	3.9760	0.2260	0.0968	0.0861	0.0188	0.0086	0.0027	458	16.2	4.72	17.59
41	3	3.8740	0.2075	0.0883	0.0876	0.0184	0.0061	0.0026	433	15.5	4.55	18.67
42	3	3.9858	0.2777	0.0927	0.0887	0.0187	0.0062	0.0026	423	14.4	4.90	14.35
43	3	3.9336	0.2053	0.0868	0.0897	0.0185	0.0061	0.0026	421	15.2	4.61	19.16
44	3	4.1516	0.2383	0.0910	0.0907	0.0193	0.0062	0.0027	413	14.4	4.93	17.42
45	3	3.8781	0.1998	0.0811	0.0917	0.0184	0.0061	0.0026	400	15.4	4.53	19.41
46	3	3.9489	0.2787	0.0969	0.0930	0.0186	0.0062	0.0026	445	14.6	4.86	14.17
47	3	4.1021	0.1132	0.0860	0.0990	0.0191	0.0059	0.0027	429	15.9	4.47	36.23
48	3	4.5399	0.1503	0.1015	0.0996	0.0205	0.0060	0.0027	450	14.3	5.03	30.20
49	3	3.9053	0.2509	0.0919	0.1004	0.0185	0.0061	0.0026	434	14.9	4.73	15.57
50	3	4.1705	0.2144	0.0950	0.1025	0.0194	0.0061	0.0026	435	14.5	4.87	19.45
51	3	4.0738	0.0979	0.0898	0.1030	0.0190	0.0059	0.0027	456	16.3	4.40	41.59
52	3	3.9473	0.2188	0.0904	0.1034	0.0186	0.0061	0.0026	433	15.1	4.66	18.04
53	3	4.0605	0.1189	0.0849	0.1038	0.0190	0.0060	0.0027	426	16.0	4.45	34.15
54	3	3.9419	0.1037	0.0886	0.1044	0.0186	0.0060	0.0027	462	16.8	4.28	38.02

Tab. 3 continued

Analysis number	Sample	Th (wt. %)	U (wt. %)	Pb (wt. %)	Y (wt. %)	Th (1σ)	U (1σ)	Pb (1σ)	Age (Ma)	Error (Ma)	Th*	Th/U
55	3	4.0670	0.2106	0.0866	0.1046	0.0190	0.0061	0.0026	407	14.7	4.76	19.31
56	3	4.1271	0.1088	0.0901	0.1069	0.0192	0.0059	0.0027	448	16.0	4.48	37.92
57	3	4.0643	0.1068	0.0854	0.1071	0.0190	0.0059	0.0026	432	16.0	4.41	38.07
58	3	4.0575	0.1080	0.0865	0.1072	0.0190	0.0060	0.0027	438	16.2	4.41	37.56
59	3	4.3006	0.1042	0.0902	0.1078	0.0197	0.0060	0.0027	434	15.4	4.64	41.27
60	3	4.3207	0.1631	0.0882	0.1095	0.0198	0.0061	0.0027	406	14.6	4.85	26.49
61	3	4.1240	0.0909	0.0903	0.1101	0.0192	0.0059	0.0026	455	16.1	4.42	45.39
62	3	4.3284	0.2547	0.0988	0.1108	0.0198	0.0062	0.0027	428	13.8	5.16	16.99
63	3	4.1417	0.1024	0.0944	0.1123	0.0191	0.0059	0.0026	470	15.9	4.48	40.46
64	3	4.1249	0.1132	0.0924	0.1158	0.0192	0.0060	0.0027	459	16.0	4.50	36.45
65	3	4.2321	0.0996	0.0951	0.1205	0.0195	0.0059	0.0026	465	15.7	4.56	42.49
66	3	4.0987	0.1257	0.0909	0.1239	0.0191	0.0060	0.0027	450	15.9	4.51	32.62
67	3	4.3022	0.1055	0.0901	0.1299	0.0198	0.0060	0.0027	433	15.4	4.65	40.78
68	3	3.9838	0.1114	0.0853	0.1300	0.0188	0.0060	0.0027	438	16.4	4.35	35.77
69	3	4.0692	0.3343	0.1086	0.1316	0.0187	0.0061	0.0026	469	13.7	5.17	12.17
70	3	4.0157	0.1162	0.0874	0.1399	0.0188	0.0059	0.0027	444	16.2	4.40	34.55
71	3	4.2227	0.1158	0.1010	0.1428	0.0195	0.0060	0.0027	489	16.0	4.60	36.46
72	3	4.0218	0.1205	0.0888	0.1527	0.0189	0.0060	0.0027	448	16.2	4.42	33.36
73	3	4.0267	0.1045	0.0852	0.1614	0.0188	0.0059	0.0026	435	16.1	4.37	38.54
74	3	4.0220	0.1214	0.0859	0.1639	0.0189	0.0060	0.0027	434	16.1	4.42	33.12
75	3	3.4540	0.1402	0.0803	0.1669	0.0171	0.0060	0.0027	458	18.3	3.91	24.63
76	3	4.2145	0.1259	0.0889	0.1670	0.0195	0.0059	0.0026	429	15.2	4.63	33.47
77	3	4.1693	0.1202	0.0931	0.1694	0.0193	0.0060	0.0027	455	15.9	4.56	34.68
78	3	4.1075	0.1306	0.0878	0.1724	0.0191	0.0060	0.0027	432	15.7	4.54	31.46
79	3	4.1026	0.4984	0.1143	0.1903	0.0188	0.0064	0.0026	445	12.4	5.74	8.23
80	3	4.3950	0.0960	0.0894	0.2011	0.0200	0.0085	0.0027	424	15.9	4.71	45.77
81	3	4.6462	0.1151	0.0946	0.2090	0.0208	0.0060	0.0027	420	14.2	5.02	40.37
82	3	4.8090	0.1404	0.1003	0.2100	0.0214	0.0060	0.0027	425	13.7	5.27	34.25
83	3	4.3890	0.1039	0.0944	0.2122	0.0200	0.0060	0.0027	445	15.3	4.73	42.25
84	3	4.8774	0.1450	0.1062	0.2130	0.0216	0.0061	0.0027	443	13.6	5.35	33.63
85	3	4.2207	0.1050	0.0936	0.2165	0.0195	0.0085	0.0027	457	16.6	4.57	40.18
86	3	4.6104	0.1174	0.0941	0.2196	0.0207	0.0059	0.0027	421	14.3	4.99	39.26
87	3	4.3192	0.1530	0.0980	0.2232	0.0198	0.0061	0.0027	454	15.1	4.82	28.23
88	3	4.8253	0.1467	0.1011	0.2267	0.0215	0.0061	0.0027	425	13.6	5.31	32.89
89	3	4.0807	0.1498	0.0893	0.2276	0.0191	0.0060	0.0027	436	15.8	4.57	27.25
90	3	4.6881	0.1170	0.0980	0.2284	0.0210	0.0060	0.0027	432	14.1	5.07	40.06
91	3	4.6693	0.1588	0.1001	0.2285	0.0209	0.0061	0.0027	431	13.8	5.19	29.40
92	3	4.6664	0.1253	0.0989	0.2298	0.0209	0.0059	0.0027	435	14.1	5.08	37.25
93	3	4.6365	0.1798	0.1037	0.2300	0.0209	0.0061	0.0027	443	13.9	5.23	25.78
94	3	4.8568	0.1222	0.0983	0.2303	0.0215	0.0085	0.0027	418	14.5	5.26	39.76
95	3	4.6095	0.1226	0.0974	0.2321	0.0207	0.0060	0.0027	434	14.3	5.01	37.59
96	3	4.8695	0.1264	0.1046	0.2340	0.0215	0.0060	0.0027	442	13.6	5.28	38.52
97	3	4.9027	0.1208	0.1035	0.2345	0.0216	0.0060	0.0027	436	13.6	5.30	40.58
98	3	4.4063	0.3078	0.1060	0.2386	0.0201	0.0063	0.0027	437	13.4	5.42	14.32
99	3	4.7007	0.1608	0.1036	0.2448	0.0210	0.0061	0.0027	442	13.9	5.23	29.24
100	3	4.3465	0.1620	0.0976	0.2493	0.0199	0.0061	0.0027	447	14.9	4.88	26.83
101	3	4.7657	0.1395	0.0994	0.2500	0.0212	0.0060	0.0027	425	13.7	5.22	34.16
102	3	4.8373	0.1370	0.1010	0.2505	0.0215	0.0060	0.0027	427	13.6	5.29	35.31
103	3	4.1995	0.1118	0.0890	0.2552	0.0195	0.0085	0.0027	435	16.6	4.57	37.57
104	3	4.2450	0.1155	0.0911	0.2572	0.0196	0.0060	0.0027	440	15.5	4.62	36.77
105	3	4.4313	0.1358	0.0975	0.2589	0.0201	0.0060	0.0027	446	14.7	4.88	32.63
106	3	4.4410	0.2677	0.1083	0.2644	0.0202	0.0062	0.0027	454	13.7	5.32	16.59
107	3	4.8920	0.1958	0.1065	0.2664	0.0217	0.0062	0.0027	430	13.1	5.53	24.99
108	3	4.4391	0.1174	0.1000	0.2665	0.0202	0.0060	0.0027	462	15.0	4.82	37.81

Tab. 3 continued

Analysis number	Sample	Th (wt. %)	U (wt. %)	Pb (wt. %)	Y (wt. %)	Th (1σ)	U (1σ)	Pb (1σ)	Age (Ma)	Error (Ma)	Th*	Th/U
109	3	4.9521	0.1880	0.1097	0.2671	0.0219	0.0062	0.0027	440	13.2	5.57	26.35
110	3	4.8785	0.1875	0.1140	0.2674	0.0216	0.0061	0.0027	463	13.4	5.49	26.02
111	3	3.9229	0.5564	0.1139	0.2826	0.0182	0.0065	0.0026	443	12.3	5.75	7.05
112	3	3.8819	0.8622	0.1378	0.2918	0.0181	0.0069	0.0027	459	10.8	6.71	4.50
113	3	3.9476	0.1754	0.0916	0.4418	0.0186	0.0060	0.0027	452	15.8	4.52	22.51
114	3	3.8594	0.2011	0.0887	1.8404	0.0183	0.0061	0.0027	438	15.8	4.52	19.19
115	3	3.9348	0.3135	0.0931	1.9532	0.0183	0.0061	0.0026	420	14.0	4.96	12.55
116	3	4.1474	0.2903	0.0951	1.9614	0.0190	0.0061	0.0026	417	13.7	5.10	14.29
117	3	3.5077	0.2423	0.0818	2.1808	0.0169	0.0059	0.0026	425	16.0	4.30	14.48
118	3	3.6272	0.2332	0.0819	2.4671	0.0173	0.0059	0.0026	417	15.7	4.39	15.55
1	64	3.9048	0.0782	0.0879	0.1184	0.0195	0.0065	0.0036	471	22.5	4.16	49.92
2	64	4.3985	0.0825	0.0900	0.0853	0.0211	0.0066	0.0036	430	20.0	4.67	53.30
3	64	4.4601	0.0853	0.0934	0.0761	0.0213	0.0066	0.0036	439	19.7	4.74	52.29
4	64	3.7798	0.0869	0.0820	0.1331	0.0191	0.0066	0.0036	450	22.7	4.06	43.49
5	64	4.4203	0.0966	0.0952	0.1452	0.0211	0.0066	0.0036	448	19.8	4.74	45.76
6	64	4.4856	0.0995	0.0956	0.1225	0.0214	0.0066	0.0036	443	19.6	4.81	45.07
7	64	3.8081	0.0999	0.0834	0.2281	0.0191	0.0066	0.0036	450	22.4	4.14	38.13
8	64	3.7678	0.1021	0.0848	0.2290	0.0190	0.0066	0.0036	461	22.6	4.10	36.91
9	64	3.8163	0.1047	0.0825	0.2469	0.0192	0.0066	0.0036	443	22.2	4.16	36.47
10	64	4.3339	0.1067	0.0902	0.1581	0.0236	0.0081	0.0044	430	24.2	4.68	40.62
11	64	3.8144	0.1074	0.0802	0.2481	0.0192	0.0066	0.0036	430	22.1	4.17	35.52
12	64	3.7950	0.1087	0.0834	0.2509	0.0191	0.0066	0.0036	448	22.3	4.15	34.92
13	64	3.6085	0.1102	0.0806	0.0774	0.0212	0.0081	0.0044	453	28.4	3.97	32.75
14	64	3.7279	0.1114	0.0761	0.2821	0.0189	0.0066	0.0036	415	22.4	4.09	33.47
15	64	4.5234	0.1114	0.0942	0.2652	0.0215	0.0066	0.0036	430	19.1	4.89	40.59
16	64	4.4759	0.1127	0.0934	0.1953	0.0213	0.0067	0.0036	430	19.4	4.85	39.73
17	64	3.7174	0.1128	0.0809	0.0796	0.0187	0.0065	0.0035	442	22.2	4.09	32.94
18	64	3.3067	0.1143	0.0799	0.1141	0.0202	0.0081	0.0044	484	30.8	3.68	28.93
19	64	4.1205	0.1149	0.0832	0.1694	0.0230	0.0081	0.0044	413	25.2	4.50	35.86
20	64	3.7117	0.1150	0.0757	0.2698	0.0188	0.0066	0.0036	413	22.4	4.09	32.27
21	64	3.7982	0.1173	0.0854	0.2411	0.0219	0.0082	0.0044	455	27.2	4.18	32.37
22	64	3.7744	0.1174	0.0817	0.2606	0.0191	0.0067	0.0036	438	22.4	4.16	32.15
23	64	4.6549	0.1175	0.0937	0.3415	0.0219	0.0067	0.0036	415	18.6	5.04	39.62
24	64	3.7956	0.1180	0.0862	0.1850	0.0219	0.0081	0.0044	460	27.3	4.18	32.18
25	64	4.7472	0.1191	0.1043	0.2834	0.0212	0.0060	0.0027	453	14.1	5.14	39.85
26	64	3.7446	0.1206	0.0780	0.2149	0.0213	0.0079	0.0043	421	26.4	4.14	31.04
27	64	3.8501	0.1208	0.0892	0.1719	0.0193	0.0067	0.0036	468	22.1	4.25	31.86
28	64	3.8271	0.1230	0.0774	0.2566	0.0192	0.0066	0.0036	409	21.6	4.23	31.12
29	64	4.7026	0.1233	0.0956	0.2728	0.0210	0.0060	0.0027	418	14.0	5.11	38.12
30	64	4.0754	0.1240	0.0904	0.2293	0.0200	0.0067	0.0036	450	20.7	4.48	32.87
31	64	4.3296	0.1253	0.0983	0.2076	0.0236	0.0082	0.0044	462	24.2	4.74	34.57
32	64	3.9266	0.1258	0.0857	0.1700	0.0219	0.0080	0.0043	441	25.6	4.34	31.21
33	64	3.4229	0.1294	0.0818	0.3051	0.0180	0.0066	0.0036	474	24.1	3.85	26.46
34	64	3.7745	0.1295	0.0765	0.2921	0.0191	0.0066	0.0036	407	21.9	4.20	29.15
35	64	3.2665	0.1304	0.0729	0.5131	0.0174	0.0066	0.0036	441	24.9	3.69	25.05
36	64	3.9003	0.1310	0.0816	0.2860	0.0195	0.0066	0.0036	421	21.2	4.33	29.77
37	64	3.8188	0.1313	0.0806	0.2658	0.0220	0.0081	0.0044	424	26.7	4.25	29.08
38	64	3.6421	0.1345	0.0788	0.1060	0.0213	0.0081	0.0044	431	27.7	4.08	27.09
39	64	3.2915	0.1386	0.0783	0.5272	0.0175	0.0066	0.0036	466	24.7	3.75	23.74
40	64	3.2657	0.1415	0.0674	0.5503	0.0174	0.0066	0.0035	404	24.2	3.73	23.08
41	64	3.3201	0.1433	0.0691	0.5641	0.0176	0.0066	0.0036	408	24.0	3.79	23.17
42	64	3.6916	0.1441	0.0877	0.2466	0.0214	0.0081	0.0044	470	27.4	4.17	25.61
43	64	3.6955	0.1445	0.0870	0.2440	0.0215	0.0082	0.0044	465	27.4	4.17	25.58
44	64	3.6445	0.1449	0.0871	0.3153	0.0184	0.0065	0.0035	471	22.3	4.12	25.15

Tab. 3 continued

Analysis number	Sample	Th (wt. %)	U (wt. %)	Pb (wt. %)	Y (wt. %)	Th (1σ)	U (1σ)	Pb (1σ)	Age (Ma)	Error (Ma)	Th*	Th/U
45	64	3.7999	0.1450	0.0813	0.2591	0.0218	0.0081	0.0044	425	26.4	4.27	26.21
46	64	3.3510	0.1480	0.0692	0.5505	0.0177	0.0066	0.0036	403	23.7	3.84	22.64
47	64	3.7819	0.1488	0.0854	0.5420	0.0191	0.0066	0.0036	446	21.6	4.27	25.42
48	64	3.3556	0.1516	0.0757	0.2285	0.0204	0.0082	0.0044	439	29.3	3.85	22.14
49	64	1.4365	0.1558	0.0397	1.3880	0.0115	0.0066	0.0035	455	45.7	1.95	9.22
50	64	3.5767	0.1567	0.0810	0.2635	0.0184	0.0067	0.0036	442	22.5	4.09	22.82
51	64	3.7825	0.1589	0.0816	0.2608	0.0218	0.0082	0.0044	424	26.2	4.30	23.81
52	64	4.7556	0.1628	0.0947	0.4799	0.0222	0.0068	0.0036	400	17.7	5.29	29.22
53	64	3.7358	0.1647	0.0867	0.2476	0.0216	0.0082	0.0044	453	26.6	4.28	22.69
54	64	3.5318	0.1664	0.0782	0.7904	0.0183	0.0067	0.0036	428	22.7	4.08	21.22
55	64	3.2855	0.2030	0.0798	0.4515	0.0175	0.0067	0.0036	451	23.3	3.95	16.18
56	64	3.1704	0.2055	0.0723	0.4799	0.0171	0.0067	0.0035	420	23.6	3.84	15.42
57	64	3.8723	0.2108	0.0903	0.3362	0.0194	0.0068	0.0036	442	20.4	4.56	18.37
58	64	3.2633	0.2184	0.0799	0.2933	0.0174	0.0067	0.0036	448	23.1	3.98	14.95
59	64	4.7271	0.2215	0.1080	0.1097	0.0222	0.0069	0.0036	442	17.4	5.45	21.34
60	64	4.0984	0.2230	0.0976	0.4122	0.0201	0.0068	0.0036	451	19.4	4.83	18.38
61	64	3.4558	0.2244	0.0778	1.1766	0.0181	0.0068	0.0036	415	22.0	4.19	15.40
62	64	3.2916	0.2251	0.0776	1.0730	0.0175	0.0068	0.0036	430	22.9	4.03	14.62
63	64	3.7036	0.2306	0.0841	0.3973	0.0189	0.0069	0.0036	421	20.8	4.46	16.06
64	64	3.2648	0.2313	0.0789	0.1967	0.0174	0.0068	0.0036	438	22.8	4.02	14.11
65	64	2.5775	0.2348	0.0636	1.4532	0.0150	0.0067	0.0035	425	26.7	3.35	10.98
66	64	3.6557	0.2355	0.0898	0.4243	0.0185	0.0067	0.0035	453	20.5	4.43	15.53
67	64	3.7203	0.2369	0.0842	0.2250	0.0189	0.0068	0.0036	418	20.6	4.50	15.70
68	64	3.9074	0.2386	0.0876	0.6938	0.0196	0.0069	0.0036	418	19.9	4.69	16.38
69	64	2.6549	0.2477	0.0705	0.1776	0.0154	0.0068	0.0035	454	26.2	3.47	10.72
70	64	2.6606	0.2486	0.0691	2.0952	0.0156	0.0069	0.0036	444	26.8	3.48	10.70
71	64	1.9425	0.2488	0.0543	1.5592	0.0131	0.0067	0.0035	441	32.3	2.76	7.81
72	64	2.6477	0.2490	0.0632	2.0467	0.0155	0.0068	0.0036	408	26.4	3.46	10.63
73	64	3.9433	0.2493	0.0941	0.2538	0.0196	0.0068	0.0036	442	19.6	4.76	15.82
74	64	3.6285	0.2501	0.0867	0.4486	0.0186	0.0069	0.0036	435	20.9	4.45	14.51
75	64	3.9672	0.2563	0.0960	0.3974	0.0197	0.0069	0.0036	446	19.4	4.81	15.48
76	64	2.5988	0.2586	0.0621	0.1742	0.0152	0.0068	0.0035	403	26.0	3.44	10.05
77	64	2.6850	0.2587	0.0743	0.2171	0.0155	0.0068	0.0035	470	25.8	3.54	10.38
78	64	4.0263	0.2592	0.0933	0.2893	0.0199	0.0069	0.0036	428	19.1	4.88	15.53
79	64	3.9225	0.2605	0.0891	0.2920	0.0196	0.0069	0.0036	417	19.4	4.78	15.06
80	64	2.8719	0.2637	0.0783	0.2083	0.0161	0.0068	0.0035	468	24.5	3.74	10.89
81	64	3.6048	0.2655	0.0891	0.2464	0.0185	0.0068	0.0036	445	20.8	4.48	13.58
82	64	2.8827	0.2675	0.0750	0.2120	0.0161	0.0068	0.0035	446	24.2	3.76	10.78
83	64	2.8299	0.2688	0.0727	0.2033	0.0160	0.0068	0.0035	438	24.4	3.71	10.53
84	64	2.6470	0.2698	0.0709	0.2046	0.0154	0.0068	0.0035	449	25.7	3.53	9.81
85	64	2.8919	0.2743	0.0805	0.2050	0.0162	0.0069	0.0036	474	24.4	3.79	10.54
86	64	2.8300	0.2745	0.0711	0.2101	0.0160	0.0068	0.0035	426	24.2	3.73	10.31
87	64	2.7991	0.2771	0.0776	0.1974	0.0159	0.0068	0.0036	467	24.8	3.71	10.10
88	64	2.8622	0.2774	0.0707	0.2323	0.0161	0.0068	0.0035	419	23.9	3.77	10.32
89	64	2.8691	0.2790	0.0764	0.7942	0.0162	0.0068	0.0036	451	24.3	3.78	10.28
90	64	2.7355	0.2800	0.0694	0.1891	0.0157	0.0068	0.0036	425	24.9	3.65	9.77
91	64	2.8178	0.2800	0.0741	0.2071	0.0160	0.0068	0.0035	443	24.3	3.74	10.06
92	64	2.5134	0.2806	0.0706	0.2088	0.0150	0.0068	0.0035	459	26.5	3.43	8.96
93	64	2.5588	0.2821	0.0647	0.2061	0.0151	0.0069	0.0035	415	25.8	3.48	9.07
94	64	2.8925	0.2822	0.0842	0.7159	0.0163	0.0069	0.0036	492	24.3	3.82	10.25
95	64	3.9721	0.2827	0.0948	0.3413	0.0197	0.0069	0.0036	433	18.8	4.90	14.05
96	64	2.7574	0.2832	0.0717	0.2176	0.0158	0.0068	0.0035	435	24.6	3.69	9.74
97	64	2.7453	0.2882	0.0704	0.1983	0.0157	0.0069	0.0036	427	24.7	3.69	9.52
98	64	2.6690	0.2892	0.0741	1.8935	0.0155	0.0069	0.0036	458	25.4	3.62	9.23

Tab. 3 continued

Analysis number	Sample	Th (wt. %)	U (wt. %)	Pb (wt. %)	Y (wt. %)	Th (1σ)	U (1σ)	Pb (1σ)	Age (Ma)	Error (Ma)	Th*	Th/U
99	64	4.1664	0.2895	0.1035	0.4168	0.0231	0.0085	0.0045	452	22.6	5.12	14.39
100	64	4.1349	0.2917	0.0951	0.8394	0.0202	0.0070	0.0036	418	18.2	5.09	14.18
101	64	2.7788	0.2923	0.0807	0.2280	0.0158	0.0069	0.0036	482	24.7	3.74	9.51
102	64	3.9843	0.2948	0.0946	1.5715	0.0197	0.0069	0.0036	427	18.9	4.95	13.51
103	64	3.7363	0.2965	0.0923	0.4642	0.0189	0.0069	0.0036	438	19.6	4.71	12.60
104	64	3.7716	0.3020	0.0887	0.3715	0.0191	0.0070	0.0036	417	19.4	4.76	12.49
105	64	2.5769	0.3024	0.0766	0.3165	0.0177	0.0084	0.0044	479	31.6	3.57	8.52
106	64	3.8512	0.3059	0.0914	0.4281	0.0194	0.0070	0.0036	421	19.3	4.85	12.59
107	64	3.7250	0.3150	0.0873	0.4149	0.0189	0.0070	0.0036	410	19.4	4.76	11.82
108	64	3.6845	0.3152	0.0926	0.4291	0.0188	0.0070	0.0036	439	19.7	4.72	11.69
109	64	4.1555	0.3218	0.1093	0.1355	0.0203	0.0070	0.0036	468	18.1	5.21	12.91
110	64	2.4775	0.3302	0.0656	1.8940	0.0147	0.0068	0.0035	413	25.0	3.56	7.50
111	64	3.7101	0.3417	0.0964	0.8700	0.0189	0.0070	0.0036	446	19.5	4.83	10.86
112	64	4.1890	0.3452	0.1093	0.1133	0.0204	0.0070	0.0036	459	17.7	5.32	12.14
113	64	3.0491	0.3519	0.0849	2.3481	0.0168	0.0070	0.0036	452	22.3	4.20	8.67
114	64	4.2054	0.3676	0.1006	0.4537	0.0203	0.0070	0.0036	416	17.0	5.41	11.44
115	64	2.9577	0.3810	0.0780	0.4634	0.0164	0.0070	0.0036	415	21.7	4.20	7.76
116	64	3.0236	0.4008	0.0803	1.7821	0.0167	0.0071	0.0036	415	21.4	4.34	7.54
117	64	1.3144	0.4041	0.0545	1.6221	0.0111	0.0070	0.0035	462	34.0	2.64	3.25
118	64	3.6469	0.4171	0.0990	0.7387	0.0187	0.0072	0.0036	441	18.7	5.01	8.74
119	64	3.5511	0.4222	0.0958	1.4226	0.0181	0.0070	0.0036	434	18.6	4.94	8.41
120	64	2.5142	0.4669	0.0711	1.6245	0.0150	0.0072	0.0036	394	22.6	4.04	5.39
121	64	3.6335	0.4680	0.1031	1.2645	0.0186	0.0072	0.0036	446	18.2	5.17	7.76
122	64	3.0916	0.4809	0.0903	2.0757	0.0168	0.0072	0.0036	433	19.8	4.67	6.43
123	64	3.1256	0.5092	0.0903	2.2131	0.0170	0.0073	0.0036	422	19.4	4.79	6.14
124	64	2.8754	0.5107	0.0881	1.2614	0.0161	0.0073	0.0036	433	20.3	4.55	5.63
125	64	3.4606	0.5364	0.0928	0.4966	0.0181	0.0074	0.0036	399	17.7	5.21	6.45
126	64	3.9972	0.5497	0.1161	0.9575	0.0198	0.0074	0.0037	448	16.4	5.80	7.27
127	64	3.5697	0.5685	0.0999	0.4646	0.0184	0.0074	0.0036	412	17.2	5.43	6.28
128	64	3.9254	0.5762	0.1283	0.1046	0.0186	0.0067	0.0027	492	12.8	5.82	6.81
129	64	3.7036	0.6547	0.1088	0.3745	0.0189	0.0076	0.0037	417	16.1	5.85	5.66
130	64	3.9168	0.6885	0.1154	0.9826	0.0196	0.0077	0.0037	419	15.4	6.17	5.69
131	64	3.3417	0.7758	0.1082	0.4038	0.0176	0.0078	0.0036	412	15.9	5.88	4.31
132	64	3.5083	0.8013	0.1144	0.2814	0.0182	0.0078	0.0036	418	15.3	6.13	4.38
133	64	2.9385	0.8124	0.1100	0.1110	0.0164	0.0078	0.0036	440	16.8	5.60	3.62
134	64	2.1517	0.8142	0.0902	0.0991	0.0139	0.0078	0.0036	420	19.2	4.82	2.64
135	64	2.8612	0.8179	0.1106	0.0898	0.0161	0.0078	0.0036	447	16.9	5.54	3.50
136	64	2.8274	0.8220	0.1029	0.0941	0.0160	0.0078	0.0036	418	16.9	5.52	3.44
137	64	2.7916	0.8285	0.1052	0.0985	0.0160	0.0079	0.0037	428	17.1	5.51	3.37
138	64	2.5158	0.8418	0.1030	0.8392	0.0150	0.0078	0.0036	438	17.7	5.28	2.99
139	64	2.8849	0.8781	0.1076	0.1134	0.0162	0.0079	0.0037	419	16.3	5.76	3.29
140	64	2.6805	0.9551	0.1144	0.9169	0.0146	0.0073	0.0027	441	12.4	5.81	2.81
141	64	2.6941	0.9767	0.1073	1.0701	0.0147	0.0073	0.0027	409	12.1	5.89	2.76
142	64	3.4190	0.9856	0.1176	1.7491	0.0169	0.0073	0.0027	397	10.8	6.64	3.47
143	64	3.1121	1.0945	0.1210	0.3997	0.0169	0.0083	0.0037	406	14.2	6.69	2.84
144	64	3.0047	1.1065	0.1325	0.9231	0.0155	0.0075	0.0027	447	11.1	6.64	2.72
145	64	3.2574	1.1508	0.1344	0.9824	0.0164	0.0076	0.0027	429	10.5	7.03	2.83
146	64	2.9457	1.4540	0.1448	0.2268	0.0164	0.0089	0.0037	422	12.4	7.71	2.03
147	64	3.2356	1.5020	0.1563	0.3468	0.0163	0.0082	0.0028	430	9.2	8.16	2.15
148	64	3.2811	1.5059	0.1540	0.2885	0.0165	0.0082	0.0028	421	9.1	8.21	2.18
149	64	3.0909	1.5306	0.1568	0.4570	0.0169	0.0090	0.0037	434	12.0	8.11	2.02

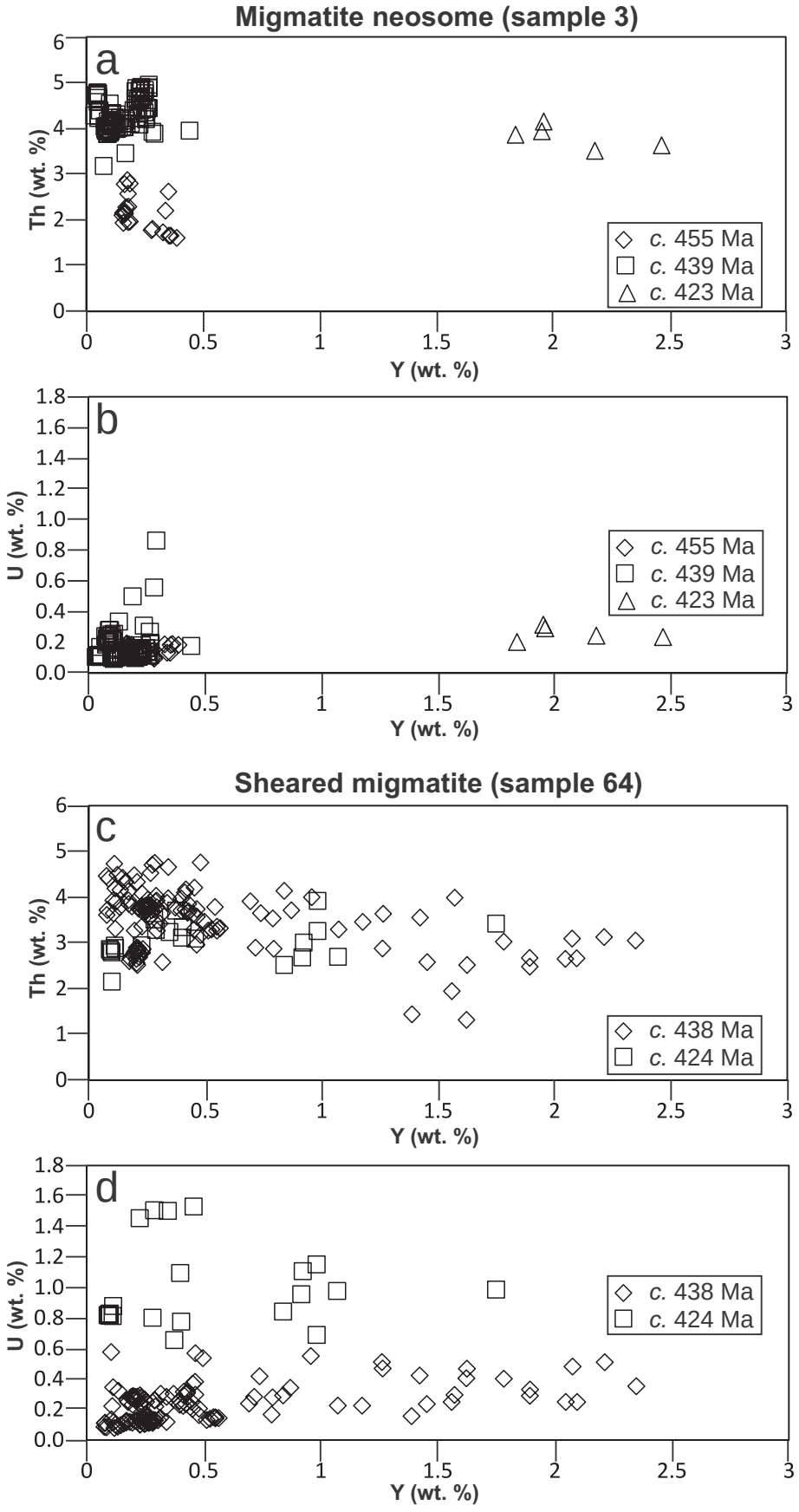

Fig. 7 Binary Th vs. Y and U vs. Y plots for monazite from migmatite neosome (**a–b**) and sheared migmatite (**c–d**).

connected with different stages of metamorphic history of the studied rocks. Moreover, a correlation between Th, U and Y content and single ages has been noticed (Tab. 3, Fig. 7). This indicates that important chemical variations were associated with monazite reconstitution and further imply that monazite may have grown (reconstituted) during specific time intervals.

6.2 Recalculation of the dating results in respect to Y–Th–U systematics and micro-textural context ("bottom-up" approach)

The variety of the "bottom-up" approach of Williams et al. (2006) was applied to test the existence of various age domains. All the results from both, the migmatite neosome and the sheared migmatite were recalculated based on the chemistry of the dated domains and their geometric position within the grains (Tab. 4).

6.2.1 Migmatite neosome

Based on Th vs. Y and U vs. Y relationships (Fig. 7a–b) and microtextural observations, three populations of monazite domains were distinguished. All of them correspond well to the relative differences in the single-spot dates, and as a consequence to the calculated average ages for the distinguished groups. The oldest population, yielding an age of 455 ± 11 Ma (n = 22, MSWD = 0.63), is characterized by low Th (<3 wt. %) and Y contents (<0.4 wt. %). The most numerous population, giving an age of 439 ± 3 Ma (n = 91, MSWD = 1.2), is characterized by higher Th (>3.1 wt. %) and low Y contents (<0.45 wt. %). The youngest and smallest population indicating an age of 423 ± 13 Ma (n = 5, MSWD = 0.34), is characterized by a strong Y enrichment (1.8–2.5 wt. %) and moderate Th contents (3.5–4.15 wt. %). It must be emphasized here that the latter results were collected solely from the cloudy core (Fig. 6b).

6.2.2 Sheared migmatite

In case of the sheared migmatite, different monazite chemical populations are not so well distinguishable like in the migmatite neosome. Nevertheless, careful examination of Th vs. Y and U vs. Y relationships (Fig. 7c–d), coupled with microtextural observations, confirms existence of at least two populations, corresponding well to the single-spot dates. This is visible on U vs. Y diagram (Fig. 7d), where obtained results are grouping in terms of U content. Monazites revealing lower U content (<0.6 wt. %) yielded an average age of 438 ± 4 Ma (n = 128, MSWD = 0.97), whereas the rest (U = 0.65–1.54 wt. %) gave an age of 424 ± 6 Ma (n = 21, MSWD = 1.09). It must be stressed that all the latter measurements were taken on tiny rims of monazites enclosed in garnets (two grains). The Th vs. Y relationships do not allow any grouping to different chemical populations. Although several e.g. low-Th outliers are visible, there is no correlation between their relatively low Th contents and age.

7. Discussion

7.1 Age of the Åreskutan migmatites

Correlation of ages and trace-element contents, along with microtextural evidence coming from petrographic study and BSE imaging, have been used here to show a protracted monazite growth in the Åreskutan migmatites. The individual domains crystallized from the prograde metamorphic phase (~455 Ma), through migmatization (~439 Ma) to late subsolidus stage probably in association with fluids induced by tectonic events (~424 Ma). We note, however, that some ages in this study were determined by using only a few grains (and a small total number of analyses) and are thus associated with relatively large 2σ errors. Clearly further detailed, preferably ion-probe dating on numerous grains is required to improve the statistics and test the validity of the obtained ages.

7.2 Tectonic implications

The evidence from the Seve Nappe Complex of northern Sweden (Norrbotten) of high-grade metamorphism of early Ordovician age (Dallmeyer and Gee 1986), perhaps starting in the late Cambrian based on Sm–Nd garnet–pyroxene–whole-rock data (Mørk et al. 1988), suggests that the subduction of the Baltoscandian outer margin may

Tab. 4 Age calculation results for selected age populations of monazite in samples 3 and 64

Sample	Population	Average age (Ma)	2s error (Ma)	MSWD
3	low Th, low Y	455	11	0.63
3	high Th, low Y	439	3	1.2
3	high Th, high Y	423	13	0.34
64	low U	438	4	0.97
64	high U	424	6	1.09

have been diachronous, starting earlier in the northern part of the mountain belt and migrating southwards during the Ordovician. Brueckner et al. (2004), and Brueckner and Van Roermund (2007) inferred that in northern Jämtland, some parts of the Seve Nappe Complex were subducted to mantle depths during the late Ordovician (*c.* 455 Ma), and rapidly exhumed in Silurian. The authors assigned this early Seve Nappe Complex evolution to a collision of Baltica with an arc or a microcontinent. Recently, additional evidence for an early to middle Ordovician event was provided by Kirkland et al. (2009), who described zircon rim growth and monazite crystallization starting at least at *c.* 470 Ma and peaking at *c.* 450 Ma in higher units of the Kalak Nappe Complex (Seve Nappe Complex equivalent) of northern Norway. Smit et al. (2010) reported a HP eclogite-facies event at 470–455 Ma (based on Lu–Hf and Sm–Nd garnet–omphacite–whole-rock data) from the Jæren Nappe in the southernmost part of the Scandinavian Caledonides, similar to that in northern Jämtland. It seems likely that these early and middle Ordovician HP events reflect multiple continent–arc (or continent–microcontinent) collisions during the closure of the Iapetus Ocean, before the Laurentia and Baltica collided.

Younger metamorphic ages (453–423 Ma) are recorded by zircon rims in a variety of lithologies of the Seve Nappes Complex in the central–northern Jämtland (Williams and Claesson 1987; Ladenberger et al. 2010, 2012; see also Tab. 1). Other workers have documented a continuous deformation evolution from Finmarkian to early Scandian (e.g., ^{40}Ar–^{39}Ar dating of Rice and Frank 2003) in the Kalak Nappe Complex. In the context of the events recorded by the Seve Nappe Complex, the oldest Åreskutan monazite ages of *c.* 455 Ma reported in this study are not substantially different from the 460–450 Ma ages from northern Jämtland given by Brueckner et al. (2004) and Brueckner and Van Roermund (2007). The chemical character of these pre-Scandian monazites suggests that they grew under high-grade subsolidus conditions, possibly related to a subduction regime along the Baltoscandian margin.

The younger, ~439 Ma monazite ages obtained in the current study are coeval with zircon rim ages from sample 3, i.e. the same rock (Ladenberger et al. 2010, 2012). Given the chemical character of the dated monazite domains, suggesting crystallization from a partial melt, this provides an important age constraint for the granulite-facies migmatization in the Seve Nappe Complex on Mt. Åreskutan. This event may well be representative of migmatization within the Seve Nappe Complex in all of Jämtland (e.g., Williams and Claesson 1987). However, this age is younger than early peak metamorphism and melting (*c.* 470–450 Ma) in the Kalak Nappe Complex recorded by zircon overgrowths in granitic dykes of the Hjelmsøy shear zone. On the other hand, it is consistent with younger U–Pb monazite ages (446 ± 3 Ma) from the same rocks (Kirkland et al. 2009).

The youngest group of monazite dates peaks at *c.* 424 Ma for the migmatite neosome and the sheared migmatite samples. In both cases fluid-assisted growth is assumed. In detail however, differences in the chemistry (mainly with regard to Y content) of these monazite domains imply that garnet was a stable phase in the sheared migmatites, whereas it was breaking down in the less deformed migmatite neosome. This agrees with the occurrence of a second generation of garnet (post thrusting) within the shear zone (Arnbom 1980) and its absence in the non-sheared migmatites.

Fluid flow is to be expected within hot shear zones (e.g., Mahan et al. 2006; Kirkland et al. 2009) and we thus interpret the ~424 Ma age of the monazite from the sheared migmatite to reflect late stages of the hot Åreskutan Nappe emplacement by thrusting along the subjacent shear zone. This suggestion is also indirectly supported by the 430 ± 3 Ma U–Pb zircon age of pegmatites occurring within the Åreskutan migmatites (Ladenberger et al. 2010). The pegmatites cross-cut the granulite-facies migmatites, but are deformed by the shear zone. Moreover the occurrence of metamorphic garnet (Arnbom 1980 and this paper) within the pegmatites implies that post-430 Ma metamorphism was likely associated with subsequent shearing. Still, it is more difficult to reconcile fluid-associated (re?)crystallization of monazite in the overlying non-sheared migmatites as the sample 3 was located approximately one hundred meters above the shear zone. One may postulate an existence of concealed, less prominent shear zones or may suggest a late-metamorphic fluid infiltration affecting the whole Åreskutan Nappe.

The ~424 Ma monazite age from Mt. Åreskutan is similar to the second peak of monazite and zircon growth in the upper parts of the Kalak Nappe Complex (Kirkland et al. 2009) showing that Scandian emplacement of the Seve Nappe Complex and its equivalents may have been contemporaneous over a large region.

8. Conclusions

The chemical monazite dating of the granulite-facies migmatites on Mt. Åreskutan (west-central Sweden) complements previous ion microprobe zircon ages of the Early Silurian peak partial melting. It provides evidence of both an earlier (Ordovician) sub-solidus history and subsequent (Late Silurian) nappe emplacement. Following conclusions can be made:

(1) Careful examination of Y– Th– U systematics and microtextures of dated monazite grains from migmatite

neosome and sheared migmatite and calculation of dates for each of the chemically characterized monazite populations document the multistage growth of this mineral at *c.* 455 Ma, 439 Ma and 424 Ma.

(2) Chemical characteristics of the various monazite domains indicate that: (a) monazite growth at *c.* 455 Ma took place under high-grade sub-solidus conditions during progressive metamorphism, possibly within a subduction tectonic regime, (b) younger, ~439 Ma monazite is interpreted to date partial melting caused by decompression and (c) the youngest monazite ~424 Ma reflects fluid-assisted growth within and around shear zones, presumably timing the thrusting within the Åreskutan Nappe.

Acknowledgements. The authors are grateful to Hans Harryson for the electron-microprobe assistance. Maciek Manecki is thanked for suggestions and discussions during dating. Early comments on the previous version of the text by Mike Williams, Peter Robinson and Peter Appel as well as reviews by Elizabeth Catlos and Fritz Finger greatly improved the quality of this manuscript. Vojtěch Janoušek is thanked for editorial handling. This study was financed by the Swedish Research Council project no. 2010-3855. J. Majka was supported by the Swedish Institute, Visby Program.

References

Albrecht LG (2000) Structural evolution of eclogite bearing nappes. Evidence from the Seve Nappe Complex, Swedish Caledonides. In: Early Structural and Metamorphic Evolution of the Scandinavian Caledonides: A Study of the Eclogite-bearing Seve Nappe Complex at the Arctic Circle, Sweden. Unpublished Ph.D. thesis. Lund University, Sweden. Ch.6, pp 1–15

Andréasson PG, Gee DG (2008) The Baltica–Iapetus boundary in the Scandinavian Caledonides and a revision of the Middle and Upper Allochthons. 33rd International Geological Congress, Oslo , EUR06601L

Andréasson PG, Gee DG, Sukotji S (1985) Seve eclogites in the Norrbotten Caledonides. In: Gee DG, Sturt BA (eds) The Caledonide Orogen – Scandinavia and Related Areas. J. Wiley & Sons, Chichester, pp 887–901

Arnbom JO (1980) The metamorphism of the Seve Nappes at Åreskutan, Swedish Caledonides. GFF 102: 359–371

Arnbom JO, Troëng B (1982) Fe–Mg partitioning between biotite and garnet from the Seve Nappe Complex, Åreskutan, Swedish Caledonides. Neu Jb Mineral, Abh 145: 34–49

Bea F, Montero P (1999) Behaviour of accessory phases and redistribution of Zr, REE, Y, Th, and U during metamorphism and partial melting of metapelites in the lower crust: an example from the Kinzigite Formation of Ivrea–Verbano, NW Italy. Geochim Cosmochim Acta 63: 1133–1153

Bingen B, Demaiffe D, Hertogen J (1996) Redistribution of rare earth elements, thorium, and uranium over accessory minerals in the course of amphibolite to granulite facies metamorphism: the role of apatite and monazite in orthogneisses from southwestern Norway. Geochim Cosmochim Acta 60: 1341–1354

Broska I, Siman P (1998) The breakdown of monazite in the West-Carpathian Veporic orthogneiss and Tatric granites. Geol Carpath 52: 79–90

Brueckner HK, Van Roermund HLM (2007) Concurrent HP metamorphism on both margins of Iapetus: Ordovician ages for eclogites and garnet pyroxenites from the Seve Nappe Complex, Swedish Caledonides. J Geol Soc, London 164: 117–128

Brueckner HK, Van Roermund HLM, Pearson NJ (2004) An Archean (?) to Paleozoic evolution for a garnet peridotite lens with Sub-Baltic Shield affinity within the Seve Nappe Complex of Jämtland, Sweden, Central Scandinavian Caledonides. J Petrol 45: 415–437

Catlos EJ, Harrison TM, Manning CE, Grove M, Rai SM (2002) Records of the evolution of the Himalayan Orogen from in situ Th–Pb ion microprobe dating of monazite: eastern Nepal and western Garhwal. J Asian Earth Sci 20: 459–479

Claesson S (1982) Caledonian metamorphism of Proterozoic Seve rocks on Mt. Åreskutan, southern Swedish Caledonides. GFF 103: 291–304

Claesson S (1987) Isotopic evidence for the Precambrian provenance and Caledonian metamorphism of high grade paragneisses from the Seve Nappes, Scandinavian Caledonides. I. Conventional U–Pb zircon and Sm–Nd whole rock data. Contrib Mineral Petrol 97: 196–204

Claesson S, Klingspor I, Stephens MB (1983) U–Pb and Rb–Sr isotopic data on an Ordovician volcanic–subvolcanic complex from the Tjopasi Group, Köli Nappes, Swedish Caledonides. GFF 105: 9–15

Dahl PS, Terry MP, Jercinovic MJ, Williams ML, Hamilton MA (2005) Electron probe (Ultrachron) microchronometry of metamorphic monazite: unravelling the timing of polyphase thermotectonism in the easternmost Wyoming Craton (Black Hills, South Dakota). Amer Miner 90: 1712–1728

Dallmeyer RD, Gee DG (1986) $^{40}Ar/^{39}Ar$ mineral age record of early Caledonian tectonothermal activity in the Baltoscandian miogeocline: implications for a polyphase Caledonian orogenic evolution. Geol Soc Am Bull 87: 26–34

Essex RM, Gromet LP, Andréasson PG, Albrecht LG (1997) Early Ordovician U–Pb metamorphic ages of the eclogite-bearing Seve Nappes, northern Scandinavian Caledonides. J Metamorph Geol 15: 665–676

Ferry JM (2000) Patterns of mineral occurrence in metamorphic rocks. Amer Miner 85: 1573–1588

Finger F, Broska I, Roberts MP, Schermaier A (1998) Replacement of primary monazite by apatite–allanite–epidote coronas in an amphibolite facies granite gneiss from the eastern Alps. Amer Miner 83: 248–258

Gee DG (1975) A geotraverse through the Scandinavian Caledonides – Östersund to Trondheim. Sve Geol Under C 717: 1–66

Gee DG, Sturt BA (eds) (1985) The Caledonide Orogen – Scandinavia and Related Areas. J. Wiley & Sons, Chichester, pp 1–1266

Gee DG, Guezou JC, Roberts D, Wolff FC (1985) The central–southern part of the Scandinavian Caledonides. In: Gee DG, Sturt BA (eds) The Caledonide Orogen – Scandinavia and Related Areas. J. Wiley & Sons, Chichester, pp 109–133

Gee DG, Juhlin C, Pascal C, Robinson P (2010) Collisional Orogeny in the Scandinavian Caledonides (COSC). GFF 132: 29–44

Gromet LP, Sjöström H, Bergman S, Claesson S (1996) Contrasting ages of metamorphism in the Seve nappes: U–Pb results from the central and northern Swedish Caledonides. GFF 118: A36–A37

Harlov DE, Hetherington CJ (2010) Partial high-grade alteration of monazite using alkali-bearing fluids: experiment and nature. Amer Miner 95: 1105–1108

Helfrich HK (1967) Ein Betrag zur Geologie des Åregebietes. Sve Geol Under C 140: 1–107

Hermann J, Rubatto D (2003) Relating zircon and monazite domains to garnet growth zones: age and duration of granulite facies metamorphism in the Val Malenco lower crust. J Metamorph Geol 21: 833–852

Högdahl K, Majka J, Sjöstrom H, Persson Nilsson K, Cleasson S, Konečný P (2012) Reactive monazite and robust zircon growth in diatexites and leucogranites from a hot, slowly cooling orogen: implications for the Palaeoproterozoic tectonic evolution of the central Fennoscandian Shield, Sweden. Contrib Mineral Petrol 163: 167–188

Jercinovic MJ, Williams ML (2005) Analytical perils (and progress) in electron microprobe trace element analysis applied to geochronology: background acquisition, interferences, and beam irradiation effects. Amer Miner 90: 526–546

Kim Y, Keewook Y, Cho M (2009) Parageneses and Th–U distributions among allanite, monazite, and xenotime in Barrovian-type metapelites, Imjingang Belt, central Korea. Amer Miner 94: 430–438

Kirkland CL, Whitehouse MJ, Slagstad T (2009) Fluid-assisted zircon and monazite growth within a shear zone: a case study from Finnmark, Arctic Norway. Contrib Mineral Petrol 158: 637–657

Kohn MJ, Malloy MA (2004) Formation of monazite via prograde metamorphic reactions among common silicates: implications for age determinations. Geochim Cosmochim Acta 68: 101–113

Kohn MJ, Wieland MS, Parkinson CD, Upreti BN (2005) Five generations of monazite in Langtang gneisses: implications for chronology of the Himalayan metamorphic core. J Metamorph Geol 23: 399–406

Konečný P, Siman P, Holický I, Janák M, Kollárová V (2004). Method of monazite dating by means of the electron microprobe. Miner Slov 36: 225–235 (in Slovak)

Krenn E, Janák M, Finger F, Broska I, Konečný P (2009) Two types of metamorphic monazite with contrasting La/Nd, Th, and Y signatures in an ultrahigh-pressure metapelite from the Pohorje Mountains, Slovenia: indications for pressure-dependent REE exchange between apatite and monazite? Amer Miner 94: 801–815

Ladenberger A, Be'eri-Shlevin Y, Gee DG, Majka J, Claesson S (2010) The origin and metamorphic history of the Seve nappes: Åreskutan Nappe, Central Caledonides, Sweden. NGF Abstracts and Proceedings 1: 103–104

Ladenberger A, Gee DG, Be'eri-Shlevin Y, Claesson S, Majka J (2012) The Scandian collision revisited – when did the orogeny start? Geophys Res Abs 14, EGU2012–12633

Mahan KH, Goncalves P, Williams ML, Jercinovic MJ (2006) Dating metamorphic reactions and fluid flow: application to exhumation of high-P granulites I a crustal-scale shear zone, western Canadian Shield. J Metamorph Geol 24: 193–217

Majka J, Budzyń B (2006) Monazite breakdown in metapelites from Wedel Jarlsberg Land, Svalbard – preliminary report. Miner Polon 37: 61–69

Majka J, Mazur S, Czerny J, Manecki M, Holm DK (2008) Late Neoproterozoic amphibolite facies metamorphism of a pre-Caledonian basement block in southwest Wedel Jarlsberg Land, Spitsbergen: new evidence from U–Th–Pb dating of monazite. Geol Mag 145: 822–830

Montel JM, Foret S, Veschambre M, Nicollet Ch, Provost A (1996) Electron microprobe dating of monazite. Chem Geol 131: 37–53

Mørk MBE, Kullerud K, Stabel A (1988) Sm–Nd dating of Seve eclogites, Norrbotten, Sweden – evidence for early Caledonian (505 Ma) subduction. Contrib Mineral Petrol 99: 344–351

Parrish RR (1990) U–Pb dating of monazite and its application to geological problems. Can J Earth Sci 27: 1431–50

Petrík I, Konečný P (2009) Metasomatic replacement of inherited metamorphic monazite in a biotite–garnet granite from Nizke Tatry Mountains, Western Carpathians, Slovakia: chemical dating and evidence for disequilibrium melting. Amer Miner 94: 957–974

Poitrasson F, Chenrey S, Shepherd TJ (2000) Electron microprobe and LA-ICP-MS study of monazite hydrothermal alteration: implications for U–Th–Pb geochronology and nuclear ceramics. Geochim Cosmochim Acta 64: 3283–3297

Pouchou JL, Pichoir F (1985) "PAP" (φρZ) procedure for improved quantitative microanalysis. In: Armstrong JT (ed) Microbeam Analysis. San Francisco Press, San Francisco, pp 104–106

Pyle JM, Spear FS (2003) Four generations of accessory-phase growth in low-pressure migmatites from SW New Hampshire. Amer Miner 88: 338–351

Pyle JM, Spear FS, Wark DA (2002) Electron microprobe analysis of REE in apatite, monazite and xenotime: protocols and pitfalls. In: Kohn ML, Rakovan J, Hughes JM (eds) Phosphates – Geochemical, Geobiological, and Materials Importance. Mineralogical Society of America Reviews in Mineralogy and Geochemistry 48: 337–362

Pyle JM, Spear FS, Cheney JT, Layne G (2005) Monazite ages in the Chesam Pond Nappe, SW New Hampshire, U.S.A.: implications for assembly of central New England thrust sheets. Amer Miner 90: 592–606

Rice AHN, Frank W (2003) The early Caledonian (Finnmarkian) event reassessed in Finnmark: $^{40}Ar/^{39}Ar$ cleavage age data from NW Varangerhalvøya, N. Norway. Tectonophysics 374: 219–236

Root DB, Corfu F (2009) Zircon U–Pb dating reveals two discrete episodes of Ordovician high-pressure metamorphism within the Seve Nappe Complex, Scandinavian Caledonides. American Geophysical Union, Fall Meeting 2009, abstract #V43D-2298

Smit AM, Scheref EE, Bröcker M, Van Roermund HLM (2010) Timing of eclogite facies metamorphism in the southernmost Scandinavian Caledonides by Lu–Hf and Sm–Nd geochronology. Contrib Mineral Petrol 159: 521–539

Spear FS, Pyle JM (2010) Theoretical modeling of monazite growth in a low-Ca metapelite. Chem Geol 273: 111–119

Spear FS, Pyle JM, Cherniak D (2009) Limitations of chemical dating monazite. Chem Geol 266: 218–230

Stephens M, Gee DG (1985) A tectonic model for the evolution of the eugeoclinal terranes in the central Scandinavian Caledonides. In: Gee DG, Sturt BA (eds) The Caledonide Orogen – Scandinavia and Related Areas. J. Wiley & Sons, Chichester, pp 953–978

Suzuki K, Adachi M (1991) Precambrian provenance and Silurian metamorphism of the Tsubonasawa paragneiss in the South Kitakami Terrane, northwest Japan, revealed by the chemical Th–U–total Pb isochron ages of monazite, zircon and xenotime. Geochem J 25: 357–376

Suzuki K, Kato T (2008) CHIME dating of monazite, xenotime, zircon and polycrase: protocol, pitfalls and chemical criterion of possibly discordant age data. Gondwana Res 14: 569–586

Terry MP, Robinson P, Hamilton MA, Jercinovic MJ (2000) Monazite geochronology of UHP and HP metamorphism, deformation, and exhumation, Nordøyane, Western Gneiss Region, Norway. Amer Miner 85: 1651–64

Törnebohm AE (1888) On the problem of the mountains (Om fjällproblemet). GFF 10: 328–336 (in Swedish)

Williams IS, Claesson S (1987) Isotopic evidence for the Precambrian provenance and Caledonian metamorphism of high grade paragneisses from the Seve nappes, Scandinavian Caledonides, II. Ion microprobe zircon U–Th–Pb. Contrib Mineral Petrol 97: 205–217

Williams ML, Jercinovic MJ, Goncalves P, Mahan KH (2006) Format and philosophy for collecting, compiling, and reporting microprobe monazite ages. Chem Geol 225: 1–15

Williams ML, Jercinovic MJ, Hetherington CJ (2007) Microprobe monazite geochronology: understanding geologic processes by integrating composition and chronology. Ann Rev Earth Planet Sci 35: 137–175

Wing BA, Ferry JM, Harrison TM (2003) Prograde destruction and formation of monazite and allanite during contact and regional metamorphism of pelites: petrology and geochronology. Contrib Mineral Petrol 145: 228–250

Yngström S (1969) Metamorphic Bedrock of the Åre Area (Åretraktens metamorfa berggrund). Unpublished Ph.D. thesis, Stockholms Universitet, Stockholm, pp 1–68 (in Swedish)

Zhou XK, O'Nions RK (1999) Monazite chemical composition: some implications for monazite geochronology. Contrib Mineral Petrol 137: 351–363